AIRCRAFT DEPARTURE RESISTANCE PREDICTION USING STRUCTURED SINGULAR VALUES

by

Brent W. York

Thesis Submitted to the Faculty of the
Virginia Polytechnic Institute and State University
in partial fulfillment of the requirements for the degree of
Master of Science
in
Aerospace Engineering

APPROVED:

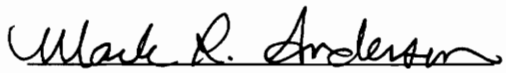

Dr. M.R. Anderson

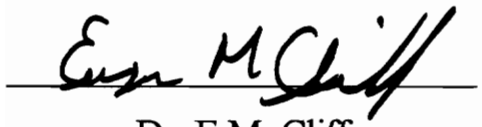

Dr. E.M. Cliff

Dr. W.C. Durham

May, 1993

Blacksburg, Virginia

AIRCRAFT DEPARTURE RESISTANCE PREDICTION USING STRUCTURED SINGULAR VALUES

by

Brent W. York

Committee Chairman: Dr. M.R. Anderson

Department of Aerospace and Ocean Engineering

(ABSTRACT)

Research has been conducted in recent years to determine the dynamic behavior of aircraft in unusual flight attitudes, particularly at very high angle-of-attack or post-stall conditions. The possibility that future advanced fighter aircraft will have the ability to perform controlled maneuvers at such attitudes is indicated by the current military aircraft flying qualities specification, MIL-STD-1797. As it becomes more important to understand the dynamics of aircraft at such flight conditions, the need for a meaningful and useful assessment of aircraft departure resistance in varying attitudes will increase proportionally. This thesis surveys some of the measures of departure susceptibility currently in use and examines a candidate for a new departure resistance criterion which offers distinct advantages over the traditional metrics.

The new departure resistance criterion, called DP_{SSV}, is essentially a measure of how much uncertainty the nominally stable plant can tolerate before being driven unstable. DP_{SSV} is calculated using structured singular values. In this thesis, DP_{SSV} is calculated over various flight conditions for a typical high-performance fighter aircraft which is represented by a full six degree of freedom, nonlinear simulation. The results are compared with those obtained by using a traditional departure susceptibility metric and by examining the eigenvalues of linearized forms of the aircraft model.

The new criterion DP_{SSV} is shown to provide more information about the departure susceptibility of an aircraft than $C_{n_{\beta_{DYN}}}$, a traditional metric, and to produce results in good agreement with the eigenvalue analysis of the stability of the aircraft for the conditions studied. The interpretation of DP_{SSV} is discussed, and suggestions for future investigation are also presented.

Acknowledgements

First, I would like to thank Dr. Mark R. Anderson for his invaluable advice, guidance, and assistance in the preparation of this thesis.

I am deeply indebted to my parents, Melvin R. and Connie J. York, for their support and encouragement throughout my college studies.

Thanks are also due to Dr. W.C. Durham and Dr. E.M. Cliff for agreeing to serve as committee members, and to Dr. F.H. Lutze for assistance above and beyond the call of duty.

Table of Contents

List of Tables

List of Figures

List of Symbols

A, B, C, D	Linear state space model matrices
$AADP$	Traditional departure resistance metric — Aileron-Alone Divergence Parameter (1/degrees)
b	Aircraft wing span (feet)
C_{l_α}	Coefficient of aerodynamic rolling moment due to angle of attack (1/degrees)
C_{l_β}	Coefficient of aerodynamic rolling moment due to sideslip (1/degrees)
$C_{l_{\delta_a}}$	Coefficient of aerodynamic rolling moment due to lateral control (1/degrees)
$C_{l_{\delta_r}}$	Coefficient of aerodynamic rolling moment due to directional control (1/degrees)
C_{m_α}	Coefficient of aerodynamic pitching moment due to angle of attack (1/degrees)
$C_{m_{\alpha_{COP}}}$	One of Kalviste's Criteria — coupled parameter analogous to the coefficient of aerodynamic pitching moment due to angle of attack
$C_{m_{\alpha_{DYN}}}, C_{m_{\beta_{DYN}}}, C_{n_{\alpha_{DYN}}}$	Dimensional stability parameters used by Kalviste
C_{m_β}	Coefficient of aerodynamic pitching moment due to sideslip (1/degrees)
C_{n_α}	Coefficient of aerodynamic yawing moment due to angle of attack (1/degrees)
C_{n_β}	Coefficient of aerodynamic yawing moment due to sideslip (1/degrees)
$C_{n_{\beta_{APPARENT}}}$	Traditional departure resistance metric — $C_{n_{\beta_{DYN}}}$ with explicit treatment of control surface effects (1/degrees)
$C_{n_{\beta_{COP}}}$	One of Kalviste's Criteria — coupled parameter analogous to the coefficient of aerodynamic yawing moment due to sideslip

$C_{n_{\beta_{DYN}}}$	Traditional departure resistance metric — approximation to the undamped natural frequency of the Dutch roll mode (1/degrees)
$C_{n_{\delta_a}}$	Coefficient of aerodynamic yawing moment due to lateral control (1/degrees)
$C_{n_{\delta_r}}$	Coefficient of aerodynamic yawing moment due to directional control (1/degrees)
$\bar{c}$	Aircraft mean aerodynamic chord (feet)
D	Scaling matrix
$\overline{D}$	Set of matrices used in defining μ (see text)
d	Parameter used in defining Kalviste's Criteria; Parameter used in determining scaling matrix D
d_i	Any positive real number, used in defining μ
d_1, d_2	Parameters used in determining scaling matrix D
DP_{SSV}	Proposed departure resistance metric — Departure Parameter based on Structured Singular Values
E, F	Pre- and postmultiplier matrices
f	Trim algorithm cost function
h	Altitude (feet)
I_n	Identity matrix of size n
$I_{xx}, I_{yy}, I_{zz}, I_{xz}$	Moments and cross moments of inertia of aircraft about stability axes (slug feet^2)
j_i	Arbitrary integer
K	Kalviste's coupling parameter
$K(s)$	Transfer function matrix of controller
k_1, k_2	Multipliers used in defining $LCDP$
$LCDP$	Traditional departure resistance metric — Lateral Control Departure Parameter (1/degrees)
L_p, L_r	Aerodynamic rolling moments due to roll rate and yaw rate (1/seconds)

L_β, L_δ	Aerodynamic rolling moments due to sideslip and total control (1/seconds^2)
M	Transfer function matrix from uncertain inputs to uncertain outputs
m_i	Dimension of Δ_i
N_p, N_r	Aerodynamic yawing moments due to roll rate and yaw rate (1/seconds)
N_β, N_δ	Aerodynamic yawing moments due to sideslip and total control (1/seconds^2)
p	Roll rate (degrees/second)
q	Pitch rate (degrees/second); Number of unique uncertainties
$\bar{q}$	Dynamic pressure (pounds/feet^2)
R_x, R_z	Moment of inertia ratios
r	Yaw rate (degrees/second)
S	Aircraft reference wing area (feet^2)
T_L	Thrust, left engine (pounds)
T_R	Thrust, right engine (pounds)
T_{SSV}	Instability period associated with DP_{SSV} (seconds)
u	Control vector
V	Velocity (feet/second)
X, Y	Parameters used in defining Kalviste's Criteria
X_∞, X_∞^R	Sets of matrices used in defining μ (see text)
x	State vector
Y_p, Y_r	Aerodynamic side force variation with roll rate and yaw rate (feet/second)
Y_β	Aerodynamic side force variation with sideslip (feet/second^2)
y	Output vector
α	Angle of attack (degrees)

β	Sideslip angle (degrees)
Δ	Uncertainty matrix
Δ_i	*i*th subblock of uncertainty matrix
ΔA	Matrix containing uncertainties in A matrix
δ	Uncertainty; Overall control deflection
δ_a	Aileron deflection (lateral control) (degrees)
δ_h	Symmetrical elevator deflection (longitudinal control) (degrees)
δ_r	Rudder deflection (directional control) (degrees)
λ_i	*i*th eigenvalue of matrix
μ	Structured singular value
μ_c	Complex-variation structured singular value
μ_r	Real-variation structured singular value
π	Throttle command (degrees)
σ	Singular value
$\bar{\sigma}$	Maximum singular value
Φ	Set of permutation matrices
ϕ	Bank angle (degrees)
ω	Angular frequency (radians/second)
ω_{SSV}	Instability frequency associated with DP_{SSV} (radians/second)
0	Subscript — nominal value

1. Introduction

Research conducted in recent years by various government agencies, including the United States Navy and the National Aeronautics and Space Administration, has increasingly involved the performance of controlled maneuvers by aircraft near or even beyond the stall angle of attack. The Navy's F/A-18 HARV program and the DARPA-sponsored X-31A Technology Demonstrator program seek to add to the understanding of aircraft dynamics at high angles of attack, and to investigate means for positive control of vehicles operating under such conditions.[1-3] Other investigations have stressed the importance of considering the extreme nonlinearity of the effects of non-zero sideslip on the aerodynamics of aircraft at high angles of attack, and the need to be able to predict more accurately the likelihood of an aircraft in a given attitude to experience uncommanded or uncontrollable motion, known as a *departure* condition.[4] The need for a better comprehension of the dynamics of aircraft operating in such a fashion very near an instability boundary, or close to departure, is paramount. One of the primary design goals in the development of recent models in the F-series of fighter aircraft has been the production of a more departure resistant vehicle.[5] The current military aircraft flying qualities specification, MIL-STD-1797, emphasizes the importance of departure resistance for military aircraft, particularly for those expected to perform maneuvers at high angles of attack.[6]

As existing programs are expanded and new studies are commissioned that require aircraft to be operated in conditions prone to departure, the need for a clearer understanding and a more reliable prediction of the departure characteristics of the aircraft will become even more important. Seltzer and Rhodeside[5] indicate that a more accurate definition of the post-stall region is needed to aid further high angle-of-attack agility research. The goal of the present research is to formulate a useful and reliable method of measuring how "close" to a departure condition an aircraft is operating, thereby contributing to the understanding of near-departure and post-stall dynamics.

Several metrics currently exist that attempt to quantify an aircraft's susceptibility to departure at a given flight condition. These include $C_{n_{\beta_{DYN}}}$, *AADP*, *LCDP*, $C_{n_{\beta_{APPARENT}}}$, and Kalviste's Criteria, among others. All of these quantities have proven to be useful in the evaluation and design of aircraft; yet, many were developed more than three decades ago. Changing aircraft capabilities and new methodologies in aircraft design lend support to the notion that new methods of quantifying an aircraft's departure resistance can and should be investigated. In a recent survey report, Seltzer and Rhodeside indicate that it is important at this point to seek

> parameters analogous to $C_{n_{\beta_{DYN}}}$ such that the maneuvering stability regions...can be predicted for an aircraft configuration...without directly calculating the bare airframe eigenvalues. By accomplishing this, this open-loop departure susceptibility criterion could aid the aircraft designer in terms of tailoring aircraft aerodynamics for the maneuvering flight conditions expected of the aircraft.[5]

A new departure resistance metric is proposed herein which addresses the limitations of the traditional measures and seeks to meet the needs described by Seltzer and Rhodeside. This new metric, called DP_{SSV}, uses methods from recent modern robust control theory as a means to estimate the susceptibility of the vehicle to departure at a given flight condition. This estimate is obtained by examining and interpreting the structured singular values of part or all of the aircraft model. All nonlinearities inherent in the model are taken into account by varying the operating parameters of the aircraft. The technique used to calculate DP_{SSV} allows for the inclusion and analysis of control systems, pilot loop closures, unusual or experimental control effectors, and so forth. Thus, the new metric shows promise for control system design with the intent to provide positive control throughout as much of the aircraft's flight envelope as possible, and is usable in current control system design methodologies. Further, the use of recently developed algorithms allows DP_{SSV} to be calculated without excessive difficulty, and its results would seem to be easier to interpret with consistency than many of the traditional metrics.

2. Background

2.1. Survey of Traditional Departure Resistance Metrics

Johnston and Hogge define *departure* broadly as "uncommanded and/or uncontrollable motion of the aircraft."[4] Seltzer and Rhodeside describe a departure as "the event in the post-stall flight regime that precipitates entry into a post-stall gyration, spin, or deep stall condition," or, more succinctly, as synonymous with "complete loss of control."[5] Several papers from the research literature surveyed below use more precise meanings for the term departure; for some research only spins were classified as departures, for others roll reversals and other such phenomena were explicitly included within the definition. However departure is defined, it always involves the inability of the pilot to control or to correct aircraft motion, a most undesirable situation particularly in combat, where the aircraft is most likely to be flown near the limits of its capabilities. The desire to quantify and to classify further the departure susceptibility of aircraft is important as work is being performed to broaden aircraft flight limits.

Early efforts regarding the prediction of aircraft departure characteristics focused on identifying which aerodynamic characteristics of the vehicle are useful for studying and predicting the phenomenon. For example, Bihrle[7] investigated the motion of an aircraft in a spin and its relation to certain bare airframe aerodynamic derivatives. A computer simulation was used to investigate aircraft motion upon entering a spin by varying each of the static, rotary, and acceleration aerodynamic derivatives. The effect of varying each quantity was classified as appreciable, significant, or insignificant for various types of spins and airframe mass distributions. By this brute force method, Bihrle was able to conclude that the yawing moment characteristics associated with the lateral control ($C_{n_{\delta a}}$) and the effective dihedral (C_{l_β}) were most important in determining the nature of a spin. Bihrle hoped that these insights would allow researchers to "identify aerodynamic fixes that are most likely to act as antispin devices" and "conceive of automatic control techniques for

spin prevention or spin recovery."[7] These are important applications for the present research.

In later work along with Barnhart,[8] Bihrle further examined the departure properties of various aircraft by plotting C_{n_β} vs. C_{l_β}. A nonlinear aircraft simulation was caused to execute a severe departure-inducing maneuver, and the time histories of several runs of this maneuver were examined to determine the characteristics of the resulting departure. Four regions were identified on each $C_{n_\beta} - C_{l_\beta}$ plot, corresponding to conditions conducive to departure, roll reversal, long excursion, or no departure. Figure 1 shows generic departure boundaries for fighters with proverse $C_{n_{\delta_a}}$. Similar graphs were produced by Bihrle and Barnhart for other cases.

Several years earlier, Moul and Paulson[9] had prepared a paper for the National Advisory Committee for Aeronautics describing the use of two criteria, $C_{n_{\beta_{DYN}}}$ and *LCDP*, in the investigation of the dynamic behavior of aircraft. The first quantity is an approximation to the undamped natural frequency of the Dutch roll mode and is defined by Moul and Paulson as

$$C_{n_{\beta_{DYN}}} = C_{n_\beta} - \frac{I_{zz}}{I_{xx}} \alpha C_{l_\beta}. \tag{2.1}$$

Moul and Paulson state that a negative value of $C_{n_{\beta_{DYN}}}$ indicates a divergence possibility.

The Lateral Control Departure Parameter, *LCDP*, defines the necessary condition for the roll angle to lateral control transfer function to be minimum phase, *i.e.*, for all its zeros to be located in the left half-plane.[5] It has three different definitions, depending upon how the control surfaces of the aircraft are used to maintain a zero bank angle. When aileron alone is used, the definition is

$$LCDP = C_{n_\beta} - C_{l_\beta} \frac{C_{n_{\delta_a}}}{C_{l_{\delta_a}}}. \tag{2.2}$$

This definition is also often called *AADP*, or the Aileron Alone Divergence Parameter. For the use of aileron plus rudder proportional to the sideslip angle ($\delta_r = -k_1 \beta$),

$$LCDP = C_{n_\beta} - C_{l_\beta} \frac{C_{n_{\delta_a}}}{C_{l_{\delta_a}}} + k_1 \left(C_{l_{\delta_r}} \frac{C_{n_{\delta_a}}}{C_{l_{\delta_a}}} - C_{n_{\delta_r}} \right). \tag{2.3}$$

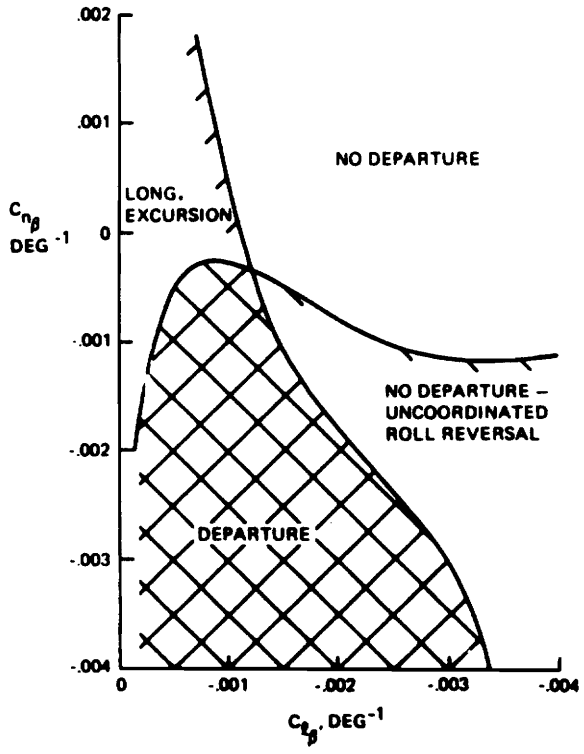

Figure 1. Example plot created by Birhle and Barnhart.

When rudder proportional to aileron is used in conjunction with the aileron deflection ($\delta_r = k_2\delta_a$),

$$LCDP = C_{n_\beta} - C_{l_\beta}\left(\frac{C_{n_{\delta_a}} + k_2 C_{n_{\delta_r}}}{C_{l_{\delta_a}} + k_2 C_{l_{\delta_r}}}\right). \tag{2.4}$$

In each case, Moul and Paulson claim that *LCDP* must remain positive to avoid a lateral divergence.

When Moul and Paulson's work was declassified, other researchers examined these departure susceptibility metrics and expanded them further. Weissman presents a slightly different definition of $C_{n_{\beta_{DYN}}}$, dispensing with the small-angle approximation used by Moul and Paulson, giving

$$C_{n_{\beta_{DYN}}} = C_{n_\beta}\cos\alpha - \frac{I_{zz}}{I_{xx}} C_{l_\beta}\sin\alpha. \tag{2.5}$$

This is the definition of $C_{n_{\beta_{DYN}}}$ which is most common and will be used for all such calculations in this research, using aerodynamic derivatives given by analysis of the bare airframe of the vehicle to be investigated.[10]

It was found by later researchers that simply requiring $C_{n_{\beta_{DYN}}} > 0$ for stability did not always give results in good agreement with experiment. Specifically, this criterion has been found inadequate for describing departure susceptibility when the subject aircraft has possible asymmetries or destabilizing external loads. In addition, the metric was determined to be inaccurate for those flight conditions where nonlinear inertial coupling moments were present, notably high angle of attack and/or nonzero sideslip attitudes.[5]

More in-depth analyses of $C_{n_{\beta_{DYN}}}$ have been performed in attempts to improve the accuracy of its predictions. Mello and Agnew[11] agree that simply ensuring that $C_{n_{\beta_{DYN}}}$ remains positive is insufficient to guarantee departure resistance throughout an aircraft's mission envelope. They recommend a minimum value of 0.004 deg^{-1} as a safety factor to ensure that the vehicle will remain departure free even under lateral weight asymmetry resulting from fuel system operation or expenditure of stores.

Skow and Titiriga[12] present results of flight tests which investigated stall behavior for steady, unaccelerated flight as a function of longitudinal control inputs only. They produced a plot of several ranges of values for $C_{n_{\beta_{DYN}}}$ and the expected stall behavior for

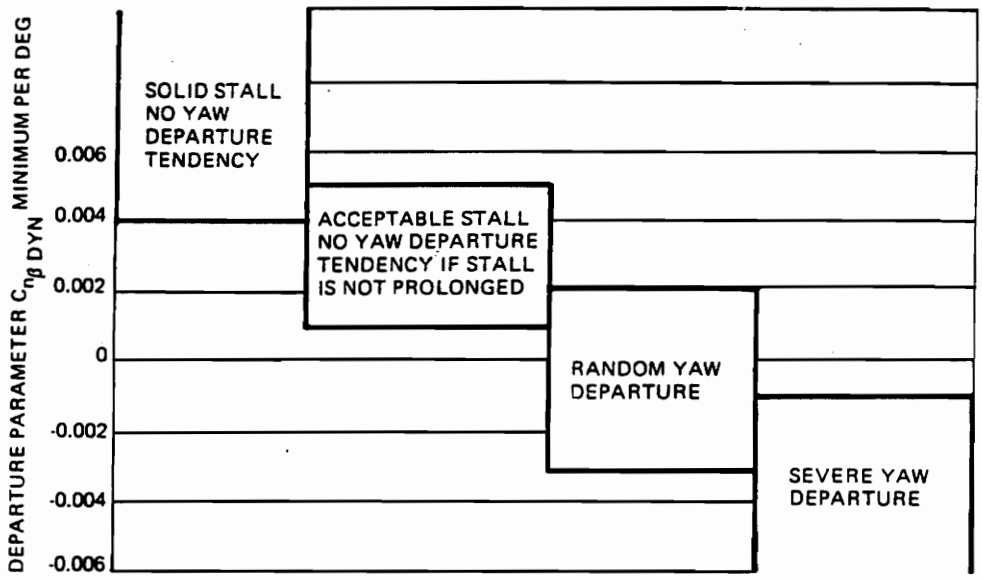

Figure 2. Expected stall behavior as function of $C_{n_{\beta_{DYN}}}$, due to Skow and Titiriga.

these values, ranging from a solid stall for $C_{n_{\beta_{DYN}}} > 0.004$ deg^{-1} to severe yaw departure for $C_{n_{\beta_{DYN}}} < -0.001$ deg^{-1} (Figure 2). However, these results do not help to classify how *resistant* to departure an aircraft is, but serve merely to help predict what type of departure will likely occur if and when departure takes place.

Bihrle insists, upon comparison of $C_{n_{\beta_{DYN}}}$ and *LCDP* with actual departure time histories, that neither is useful *by itself* as a departure resistance criterion.[8] Although $C_{n_{\beta_{DYN}}}$ correctly predicts the stability of the Dutch roll mode, it fails to take into account aerodynamic and inertial coupling with the longitudinal motion, nor does it include effects due to lateral control. Tinger confirms that, since $C_{n_{\beta_{DYN}}}$ is an open-loop parameter, it may fail to predict departures correctly when they are caused by control movements.[13] For example, at high angles of attack, large aileron deflections can produce adverse yaw of sufficient magnitude to drive the aircraft to instability, even though $C_{n_{\beta_{DYN}}}$ might remain positive. Bihrle notes as well that *LCDP*, which is derived from the simplified aircraft rolling and yawing moment equations, can be useful for predicting flight conditions conducive to roll reversal, but by itself is unable to predict reliably the susceptibility of an aircraft to departure in general.[8]

Weissman[10] plotted $C_{n_{\beta_{DYN}}}$ vs. *LCDP* and defined several regions on the resulting graph that predict various types of departure, or departure resistance. The boundaries demarcating these regions were empirically determined by analyzing time histories generated by a nonlinear, six degree-of-freedom simulation, and were later found by Weissman to agree well with actual flight test data. Weissman's graph is reproduced in Figure 3. Researchers at Northrop Corporation[14] and others later made minor modifications to the Weissman graph in efforts to improve its accuracy further. However, Tinger indicates that tests performed with data obtained from the AV-8B Harrier II showed that the revised Weissman criteria can be overly conservative in estimating the departure susceptibility boundary.[13]

Rhodeside[5] integrated the Bihrle and Weissman departure susceptibility graphs into a single plot of various departure regions, and tested the new criterion using a manned flight simulator. It was found that, while some of the identified behavior regions were reasonably accurate, many areas in the new $C_{n_{\beta_{DYN}}}$ –*LCDP* plane could not be specified to

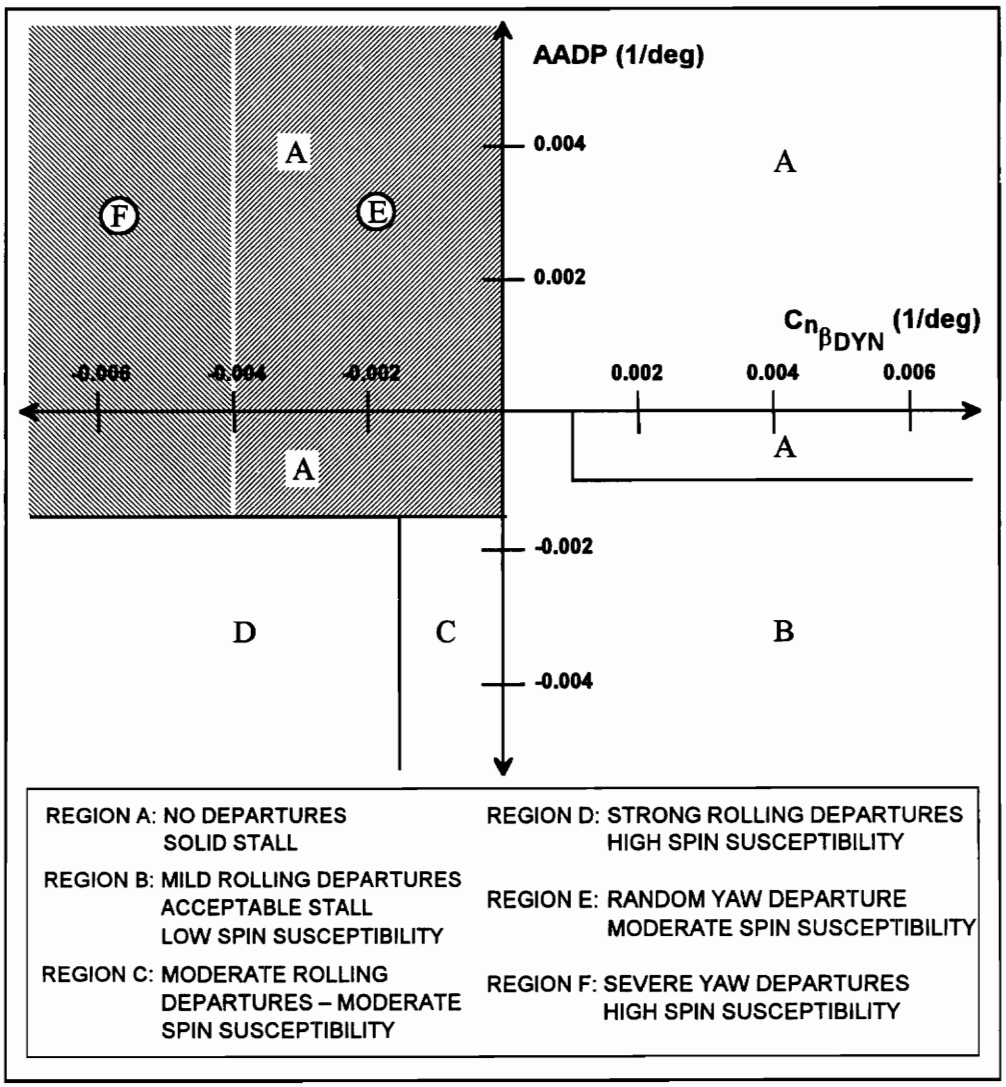

Figure 3. Weissman graph of regions of departure and spin susceptibility.

indicate any particular behavior, as the departure characteristics of the aircraft were largely dependent on properties that were not a part of the bare airframe, such as pilot technique.

Pelikan[15] describes $C_{n_{\beta_{APPARENT}}}$, a departure resistance parameter used by McDonnell Douglas in the development of the F/A-18 high angle of attack control laws. This metric is based on $C_{n_{\beta_{DYN}}}$, but includes contributions due to control surface deflections explicitly. It is defined as

$$C_{n_{\beta_{APPARENT}}} = \left(\frac{C_n(\beta)+C_n(\delta)}{\beta}\right)\cos\alpha + \left(\frac{C_l(\beta)+C_l(\delta)}{\beta}\right)\frac{I_{zz}}{I_{xx}}\sin\alpha. \quad (2.6)$$

This criterion presents some advantages over the use of $C_{n_{\beta_{DYN}}}$ in that it accounts for the effects of sideslip and lateral control deflections. Like $C_{n_{\beta_{DYN}}}$, $C_{n_{\beta_{APPARENT}}}$ should remain positive for departure resistance.

Johnston and Hogge[4] present an examination of the aerodynamic derivatives in analyzing the departure characteristics of the A-7 aircraft. They indicate that aerodynamic coupling is important in predicting the nose slice departure experienced by the A-7, and that $C_{n_{\beta_{DYN}}}$ and *LCDP* do not take such coupling into account.

Kalviste[16] has presented a more versatile set of departure resistance criteria. As with many of the previously discussed metrics, Kalviste's Criteria are derived from the aircraft equations of motion. However, in contrast to conventional stability analysis techniques, Kalviste's method does not ignore coupling between the longitudinal and lateral-directional modes of motion. This modeling detail provides Kalviste's Criteria with potentially better reliability at high angle of attack and nonzero sideslip. Inherent nonlinearities in the aircraft six degree of freedom equations of motion are included as well. Kalviste postulates that the departure characteristics of an aircraft can be approximated by its rotational motion relative to the flight path, and working from this assumption derives the following criteria. Using $C_{n_{\beta_{DYN}}}$ as given in equation (2.5) and defining

$$C_{m_{\alpha_{DYN}}} = C_{m_\alpha} - \frac{b}{\bar{c}}\left(\frac{I_{yy}}{I_{zz}}C_{n_\alpha}\sin\alpha + \frac{I_{yy}}{I_{xx}}C_{l_\alpha}\cos\alpha\right)\tan\beta, \quad (2.7a)$$

$$C_{m_{\beta_{DYN}}} = C_{m_\beta} - \frac{b}{\bar{c}}\left(\frac{I_{yy}}{I_{zz}}C_{n_\beta}\sin\alpha + \frac{I_{yy}}{I_{xx}}C_{l_\beta}\cos\alpha\right)\tan\beta, \quad (2.7b)$$

$$C_{n_{\alpha_{DYN}}} = C_{n_\alpha} \cos\alpha - \frac{I_{zz}}{I_{xx}} C_{l_\alpha} \sin\alpha, \tag{2.7c}$$

$$X = \frac{b}{I_{zz}} C_{n_{\beta_{DYN}}} - \frac{\bar{c}}{I_{yy}} C_{m_{\alpha_{DYN}}}, \tag{2.7d}$$

and

$$Y = \frac{\bar{c}b}{I_{yy} I_{zz}} \left(C_{n_{\alpha_{DYN}}} C_{m_{\beta_{DYN}}} - C_{n_{\beta_{DYN}}} C_{m_{\alpha_{DYN}}} \right), \tag{2.7e}$$

Kalviste produces an equation for the "coupling parameter,"

$$K = \text{sign}\left(X^2 - 4Y\right) \frac{I_{zz}}{b} \sqrt{\left|X^2 - 4Y\right|}, \tag{2.8}$$

and for two stability parameters $C_{n_{\beta_{COP}}}$ and $C_{m_{\alpha_{COP}}}$; if K is positive,

$$C_{n_{\beta_{COP}}} = \frac{I_{zz}}{2b} \left(X + d\sqrt{X^2 - 4Y} \right) \tag{2.9a}$$

and

$$C_{m_{\alpha_{COP}}} = \frac{I_{yy}}{2\bar{c}} \left(-X + d\sqrt{X^2 - 4Y} \right), \tag{2.9b}$$

where

$$d = \text{sign}\left(\frac{b}{I_{zz}} C_{n_{\beta_{DYN}}} + \frac{\bar{c}}{I_{yy}} C_{m_{\alpha_{DYN}}} \right), \tag{2.9c}$$

and if K is negative,

$$C_{n_{\beta_{COP}}} = \frac{I_{zz}}{b} \sqrt{Y} \tag{2.10a}$$

and

$$C_{m_{\alpha_{COP}}} = -\frac{I_{yy}}{\bar{c}} \sqrt{Y}. \tag{2.10b}$$

For stability, Kalviste indicates that

$$\begin{aligned} &K \geq 0, \\ &C_{n_{\beta_{COP}}} \geq 0, \\ &C_{m_{\alpha_{COP}}} \leq 0 \end{aligned} \tag{2.11}$$

must be satisfied. Figure 4 displays the results of applying the Kalviste Criteria to a typical aircraft configuration. This illustrates how unwieldy the *results alone* can become for an analytical solution to the departure resistance problem. Analytical solutions are useful to

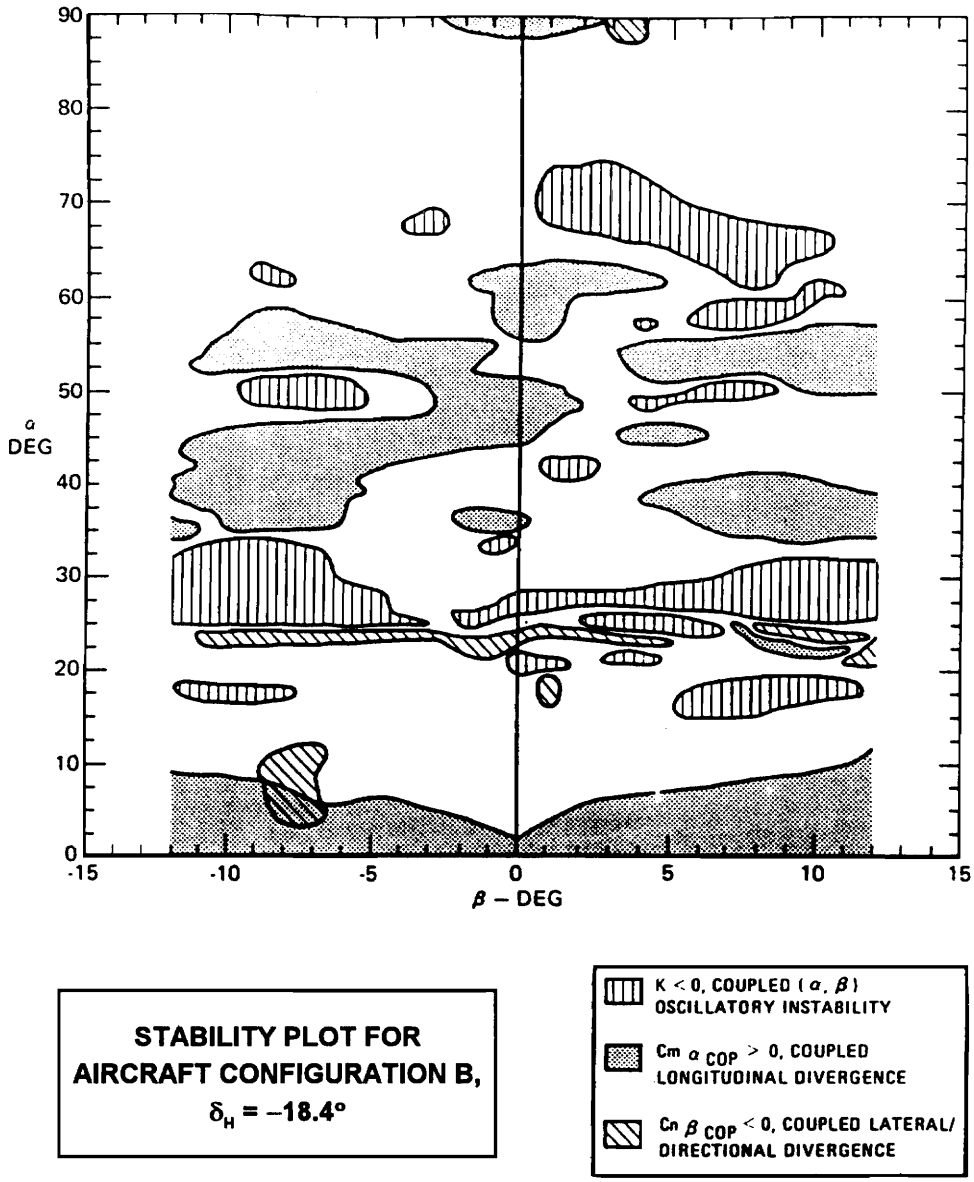

Figure 4. Predictions of Kalviste's Criteria for typical aircraft configuration.

gain insights, but are still only approximations to the complete solution. In addition, such a solution does not produce a single measure, making design applications difficult.

2.2. Motivation

The measures of aircraft departure susceptibility described previously have met with varying degrees of success in accurately predicting an imminent departure condition. Each represents a valuable contribution to the understanding of aircraft departure dynamics; however, all suffer from certain fundamental limitations.

First, all are derived from the simplified aircraft equations of motion and fail to take adequate account of the extreme nonlinearities in aerodynamic properties that are exhibited by modern fighter aircraft at high angles of attack and large sideslip angles. In fact, most treat all variations in aerodynamic quantities as strictly linear with respect to sideslip. Further, only Kalviste[16] addresses the effects of coupling between the lateral/directional and longitudinal modes. Therefore, most of these traditional criteria appear to be of limited usefulness in asymmetric and/or high angle of attack flight.

Second, and perhaps more importantly, all of the existing measures are concerned only with the bare airframe of the vehicle. Little, if any, provision is made for inclusion of the effects of a control system, the response of the pilot, or non-traditional control effectors such as vectored thrust.

Finally, the traditional departure susceptibility metrics are useful for determining the departure characteristics of a completed vehicle design and mapping existing regions of instability, but they are not readily applicable to the design of control systems for departure prevention. Calculating one or more of these traditional criteria will give the aircraft designer useful information about the current departure properties of a vehicle, but will not clearly indicate how he might go about altering these characteristics.

3. Technical Approach and Procedures

3.1. New Departure Resistance Metric

A new departure resistance metric is described which addresses many of the limitations in the traditional measures. The new parameter, DP_{SSV}, is not analytically derived from the aircraft equations of motion, but instead uses computational techniques from robust control theory to analyze the departure susceptibility of the aircraft at a given flight condition. All global nonlinearities and coupling effects are included. The state space model to be analyzed can include other relevant aircraft systems in addition to the bare airframe treated by the traditional departure resistance metrics. This new metric can be used directly in modern control system design techniques as an optimization function.[17] Designers can then develop control systems specifically to minimize departure susceptibility.

3.1.1. Robust Stability of Linear Systems

Researchers working with multiple input, multiple output (MIMO) systems saw the need for a technique whereby the stability robustness of a given MIMO system could be measured and expressed. The desire was, initially, to determine the stability of a linear system when subjected to a given magnitude of uncertainty in its parameters. Later, work was published that took the concept further by providing means for directly estimating the bounds on the uncertainty such that the system would remain stable.

Several methods have been used in the past for investigating the stability of linear systems under parametric uncertainty. For example, one procedure has been to use a Lyapunov approach to determine the allowable parameter uncertainty bounds for stability.[18,19] Though this method provides reasonable results, its usefulness as a design tool has not been widely investigated. One goal of this research is to develop a means of assessing the departure resistance of an aircraft that will yield results that a designer can

use directly to adjust and to improve the control system. A procedure showing promise for such use in the analysis of the robust stability of linear systems, as well as in design applications, is the *structured singular value.*

3.1.2. Structured Singular Values

The concept of the structured singular value was first presented by Doyle,[20] and has been examined and extended by many other researchers. The structured singular value measures the largest parametric uncertainty a given system can withstand before violating a stability condition.

Figure 5 represents a closed loop containing a system with real uncertainties.[21] M contains the dynamic characteristics of the nominal plant. The matrix Δ is block diagonal and accounts for the placement or structure of uncertainties in the feedback system. The system in M, by itself, is assumed to be stable. The object is to determine whether the closed-loop system including Δ is also stable.

The Δ of smallest "size" that will make $\det(I+M\Delta)=0$ represents the maximum uncertainty the system can accommodate before being driven to instability. The "size" of Δ is expressed as its 2-norm, defined as

$$\|\Delta\|_2 = \max_i \sqrt{\lambda_i(\Delta^* \Delta)}, \tag{3.1}$$

where λ_i represents the ith eigenvalue of the matrix, and the operator * denotes the complex conjugate transpose. The structured singular value μ is defined as the multiplicative inverse of the spectral or 2-norm of the largest allowed Δ. The formal definition of μ as given by Doyle is

$$\mu(M) = 0 \text{ if no } \Delta \in X_\infty \text{ solves } \det\left(I+M\Delta\right) = 0, \tag{3.2a}$$

else,

$$\frac{1}{\mu(M)} = \min_{\Delta \in X_\infty}\left(\bar{\sigma}(\Delta) : \det\left(I+M\Delta\right) = 0\right). \tag{3.2b}$$

For this research, X_∞ is defined as

$$X_\infty = \left\{\text{block diag}\left(\Delta_1, \Delta_2, ..., \Delta_q\right) \middle| \bar{\sigma}(\Delta_i) < 1, \Delta_i \in \mathbf{C}^{m_i \times m_i}\right\} \tag{3.3}$$

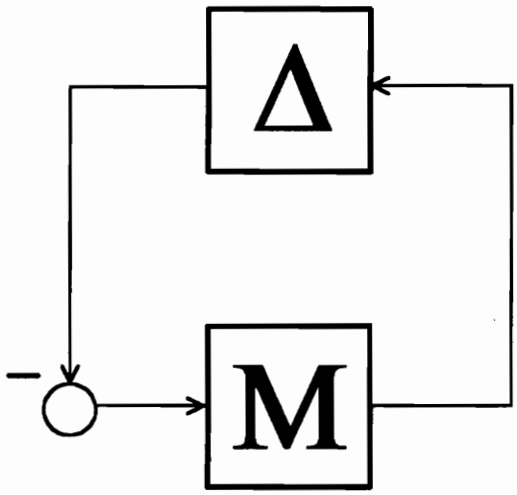

Figure 5. Closed loop representation of uncertain system.

where each Δ_i has a dimension m_i, and $\bar{\sigma}(\Delta)$ represents the maximum singular value of the given Δ, equivalent to the 2-norm of Δ:

$$\bar{\sigma}(\Delta) = \|\Delta\|_2. \tag{3.4}$$

Equation (3.2) proves to be quite difficult to solve for most systems.[21] Many local minima exist, making the minimization difficult to carry out. For this reason, Doyle also describes an upper bound for μ which proves much simpler to find. This upper bound is given by

$$\mu(M) \leq \min_{D \in \bar{D}} \left(\bar{\sigma}\left(DMD^{-1} \right) \right), \tag{3.5}$$

with

$$\bar{D} = \left\{ \text{block diag}\left(d_1 I_{m_1}, d_2 I_{m_1}, ..., d_q I_{m_q} \right) \right\}, \tag{3.6}$$

where d_i is a positive real number and I_{m_i} is the identity matrix of size m_i. The right hand side of equation (3.5) represents an optimization problem with no non-global minima and is much easier to solve. The disadvantage in using this upper bound, of course, is that the estimate of how much uncertainty a given MIMO system can handle before being driven to instability will be more conservative than necessary. However, Doyle has shown that for $q \leq 3$ (*i.e.*, for three or fewer blocks), equation (3.5) becomes an equality:

$$\mu(M) = \min_{D \in \bar{D}} \left(\bar{\sigma}\left(DMD^{-1} \right) \right). \tag{3.7}$$

Equation (3.7) can be applied to the present work, as only the case where $q = 2$ is considered.

A further point to be noted is the assumption in Doyle's definition of the structured singular value that uncertainties contained in Δ may be complex. For all cases examined in this thesis, only real variations are of interest, since the investigated uncertainties are in real-valued quantities such as stability derivatives. Thus, using Doyle's original definition would produce an overly conservative robustness measure by taking into account the effects of variations along the imaginary axis which are not needed.

Jones[22] has modified Doyle's equations for the case of strictly real-valued uncertainties. He defines the real-variation structured singular value as

$$\frac{1}{\mu_r(M)} = \min_{\Delta \in X_\infty^R} \left(\bar{\sigma}(\Delta) : \det\left(I + M\Delta\right) = 0 \right), \tag{3.8}$$

with

$$X_\infty^R = \left\{ \text{block diag}\left(\Delta_1, \Delta_2, ..., \Delta_q\right) \middle| \bar{\sigma}(\Delta_i) < 1, \Delta_i \in \Re^{m_i \times m_i} \right\}. \tag{3.9}$$

Again, the formal definition given above represents a very difficult optimization problem. Therefore, Jones has defined an analogue to equation (3.7) that applies to equation (3.9), as follows:

$$\mu_r(M) = \min_{D \in \bar{D}} \left[\max_{\Phi} \bar{\sigma} \left\{ DMD^{-1}\Phi + \left(DMD^{-1}\Phi\right)^T \right\} / 2 \right], \tag{3.10}$$

with $\bar{D}$ defined as in equation (3.6), and

$$\Phi = \text{diag}\left((-1)^{j_1} I_{m_1}, (-1)^{j_2} I_{m_2}, ..., (-1)^{j_q} I_{m_q} \right), \tag{3.11}$$

where j_i is an arbitrary integer and q and I_{m_i} are defined as before. Note that Φ serves only to change the sign of D in order to represent all possible sign combinations in Δ.

Jones and other have shown that Osborne's technique[23] can be employed to find a scaling matrix D for equation (3.10) by minimizing the Frobenius norm of DMD^{-1} instead of the maximum singular value. The Frobenius norm of a matrix A is defined as

$$\|A\|_F = \sqrt{\text{trace}\left(A^* A\right)}. \tag{3.12}$$

Since the Frobenius norm is an upper bound to the 2-norm, minimizing the Frobenius norm reduces the 2-norm, but is not guaranteed to minimize it.[21] This adds to the conservatism of the result for μ_r, but considerably lightens the computational burden. Osborne's technique can thus be used to obtain a good approximation to the right hand side of equation (3.8).

As only real parameter variations are considered in this research, the definition for μ_r given in equation (3.10) is used to calculate μ unless otherwise stated. This definition for the structured singular value is used below in the development of the new departure resistance metric.

3.1.3. Development of DP_{SSV}

The tendency of an aircraft to enter a departure is related to its behavior under variation of key model parameters, most notably certain aerodynamic derivatives.[7,24] The variation of derivatives believed to be connected to departure phenomena can cause the aircraft model to become unstable. The greater the allowable variation in such parameters without leading to instability, the greater the resistance of the aircraft to departure. Departure susceptibility is thus measured in this research as "nearness" to an instability boundary. A new metric is considered which uses the structured singular value to quantify the stability robustness of the aircraft at each flight condition with respect to variations in important stability derivatives.

The definition of DP_{SSV} is straightforward:

$$DP_{SSV} = \min_{\omega} \frac{1}{\mu(\omega)} \tag{3.12}$$

Here ω is a vector containing all positive frequencies of interest. In practice, the reciprocal of μ is calculated over the frequency range in ω and the minimum is found and stored as DP_{SSV}, while the frequency at which the minimum was attained, ω_{SSV}, is also stored for future reference. Additionally, the quantity T_{SSV} is defined to be

$$T_{SSV} = \frac{2\pi}{\omega_{SSV}} \tag{3.13}$$

and represents the period of the unstable mode of interest. For this research, T_{SSV} was stored instead of ω_{SSV} for analysis purposes.

Figure 6 illustrates the principles behind the use of structured singular values in this research. The A matrix in the state space model of the aircraft and its subsystems is altered by some ΔA, and the results are analyzed. When the system becomes unstable, then ΔA has been made as "large" as possible. The norm of the largest allowed ΔA defines the bound on uncertainty that DP_{SSV} measures.

To isolate specific components of A for analysis, the matrix ΔA is decomposed as

$$\Delta A = E \Delta F, \tag{3.14}$$

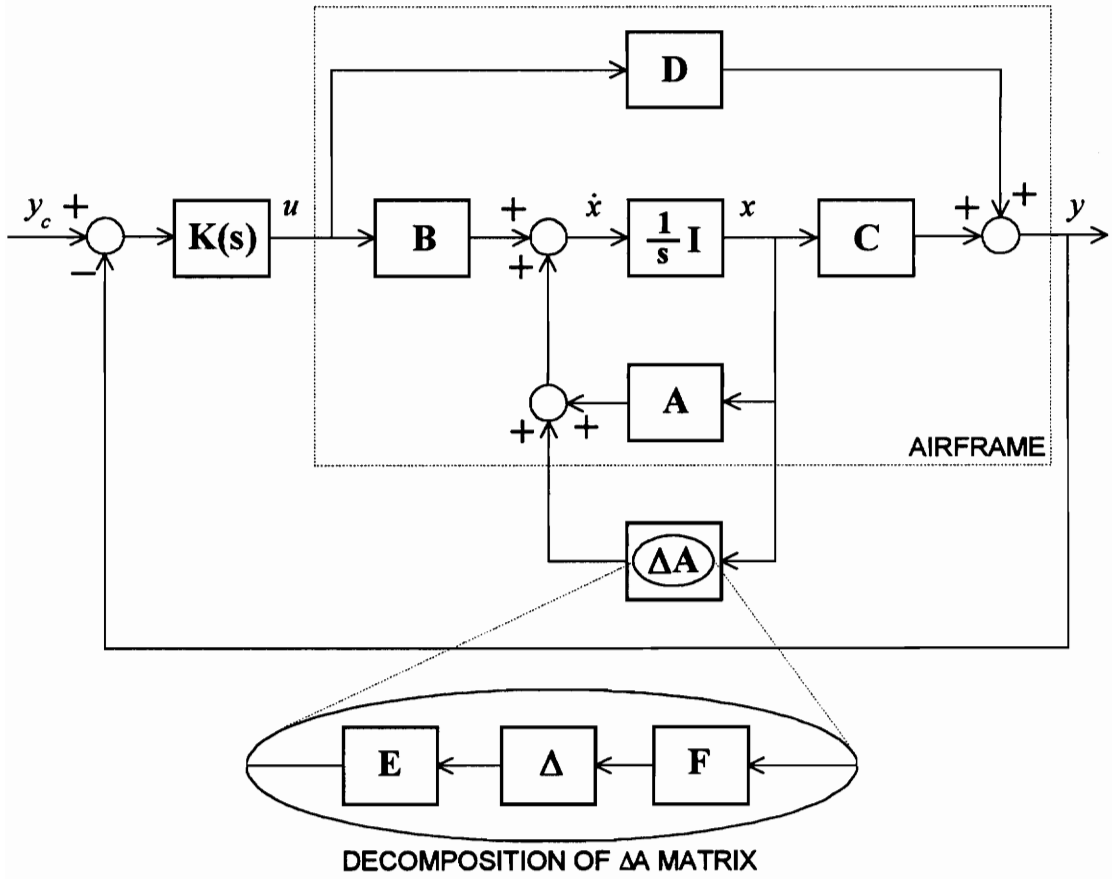

Figure 6. State space representation of **FANGS** analysis.

where Δ is an uncertainty matrix as defined in equation (3.9), and E and F are pre- and postmultiplier matrices which "interface" this matrix to the nominal A matrix. The multiplier matrices are used to select individual elements or combinations of elements from the A matrix of the aircraft's state space model. The elements or combinations thus produced are the quantities which will be subjected to uncertainty in the structured singular value analysis. Note that the M matrix shown in Figure 5 is analogous to the entire system in Figure 6 excluding the Δ matrix. Analysis of Figure 6 reveals that

$$M(s) = E\left[sI - A + B\left(I + K(s)D\right)^{-1} K(s)C \right]^{-1} F, \tag{3.15}$$

or, if $K(s) = 0$ in Figure 6,

$$M(s) = E\left(sI - A\right)^{-1} F. \tag{3.16}$$

Equation (3.16) is used in this research to find DP_{SSV} for variations in the state matrix of an aircraft model.

The definition of DP_{SSV} presented here is a rather broad one. With appropriate definition of ΔA, DP_{SSV} could be used to investigate the stability of an aircraft with respect to the variation of any or all of its parameters. In fact, this is part of the attraction of this approach. For the purposes of this research, stability with respect to variation only of the derivatives $\frac{\partial \dot{p}}{\partial \beta}$ and $\frac{\partial \dot{r}}{\partial \beta}$ will be examined as a potential indicator of departure susceptibility, but certainly other combinations of elements from the A matrix of the aircraft model could provide additional insight.

3.1.4. DP_{SSV} Example

As an example of the results produced for DP_{SSV}, a simple fourth-order model is analyzed, representing the lateral-directional characteristics of an aircraft. The state space representation, given in the form $\dot{x} = Ax + Bu$, is

$$\begin{bmatrix} \dot{p} \\ \dot{r} \\ \dot{\beta} \\ \dot{\phi} \end{bmatrix} = \begin{bmatrix} L_p & L_r & L_\beta & 0 \\ N_p & N_r & N_\beta & 0 \\ Y_p & Y_r & Y_\beta & \frac{g}{U_0} \\ 1 & 0 & 0 & 0 \end{bmatrix} \begin{bmatrix} p \\ r \\ \beta \\ \phi \end{bmatrix} + Bu. \tag{3.17}$$

The A matrix was filled with values obtained for an F-4 Phantom in a trimmed flight condition at $h = 0$ ft and $V = 224$ ft/sec.[25] For this example only, uncertainties were examined in the quantities Y_r and Y_β. These particular aerodynamic derivatives were chosen because they are expected to affect the stability of the Dutch roll mode without significantly affecting the spiral mode. This was desired since the spiral mode is nearly unstable in the nominal system (Figure 7); a better illustration of DP_{SSV} can be presented by perturbing the much more stable Dutch roll mode. The pre- and postmultiplier matrices are

$$E = \begin{bmatrix} 0 & 0 \\ 0 & 0 \\ Y_{r_0} & Y_{\beta_0} \\ 0 & 0 \end{bmatrix} \tag{3.18}$$

and

$$F = \begin{bmatrix} 0 & 1 & 0 & 0 \\ 0 & 0 & 1 & 0 \end{bmatrix}. \tag{3.19}$$

Defining

$$\Delta = \begin{bmatrix} \dfrac{\delta(Y_r)}{Y_{r_0}} & 0 \\ 0 & \dfrac{\delta(Y_\beta)}{Y_{\beta_0}} \end{bmatrix}, \tag{3.20}$$

where $\delta(\cdot)$ represents the uncertainty in the specified aerodynamic derivative, gives

$$\Delta A = E \Delta F = \begin{bmatrix} 0 & 0 & 0 & 0 \\ 0 & 0 & 0 & 0 \\ 0 & \delta(Y_r) & \delta(Y_\beta) & 0 \\ 0 & 0 & 0 & 0 \end{bmatrix}, \tag{3.21}$$

which is indeed the ΔA matrix that is required. Note that the Δ defined in equation (3.20) is normalized by the nominal stability derivatives so that the results represent percent allowable variation in the derivatives.

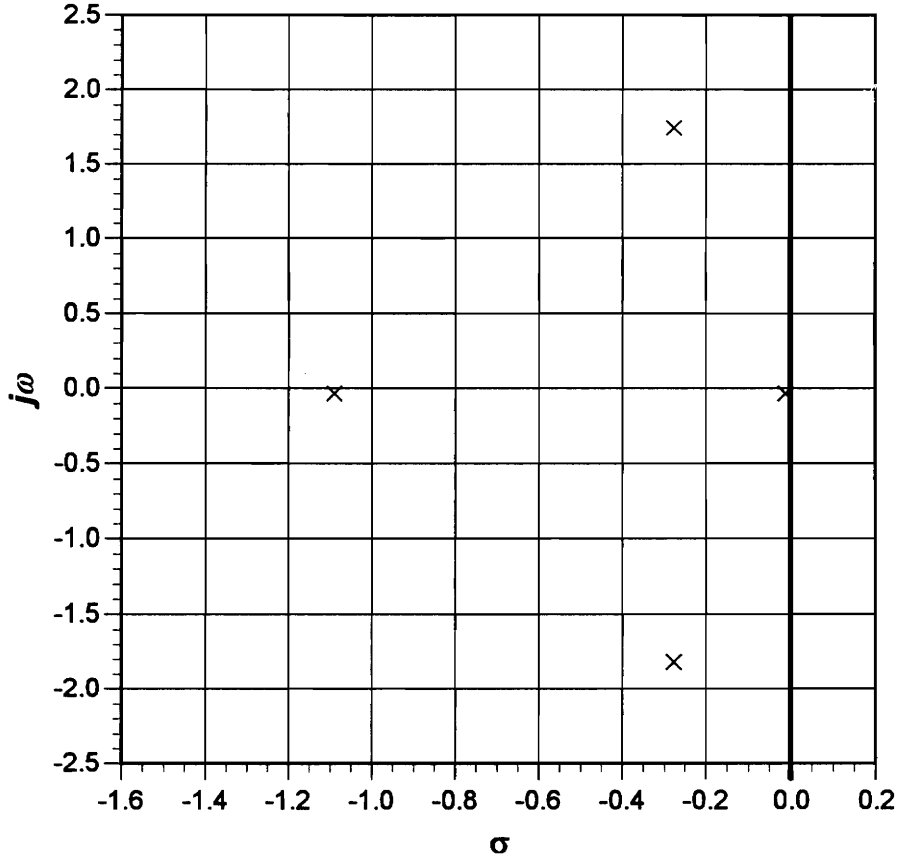

Figure 7. Eigenvalues of nominal system for example fourth-order model.

The structured singular value $\mu(\omega)$ was calculated for this example over a range of angular frequencies as shown in Figure 8. For discussion, two methods were employed to calculate μ. The dotted line labelled μ_c represents a calculation using equation (3.7), which takes into account the possibility of complex variations in the stability derivatives. The solid line identified as μ_r was produced using equation (3.10) and only allows for real-valued variations in the A matrix.

Figure 9 shows a Monte Carlo scatter plot of the eigenvalues of the A matrix, allowing up to ±83% simultaneous variation in Y_r and Y_β. This variation brings the Dutch roll mode just to the point of instability, and thus represents the exact result to be predicted by $\frac{1}{\mu}$. This corresponds to a value for μ of approximately 1.2, represented in Figure 8 by the dashed line labelled *exact*. As expected, the results shown for both μ curves in Figure 8 are quite conservative. A larger value for μ corresponds to a smaller value for its reciprocal, or a smaller expected allowable uncertainty in the aerodynamic derivatives. The maximum of the μ_c curve is located at the expected Dutch roll angular frequency of 1.78 rad/sec and corresponds to a variation limit of ±31%. The maximum of the μ_r curve is 2.18, representing an improved limit of ±46%. Both limits are conservative, but the real-valued structured singular value is considerably less conservative than its complex-valued counterpart, again as expected.

Current control system synthesis methodologies allow the use of parameters like μ_c directly in the design process. Metrics of the form of μ_r are also usable in design and are a topic of current research. Data such as that obtained from the eigenvalue scatter plot in Figure 9 are important for analysis purposes but difficult to utilize directly in design procedures.

3.2. Case Study

The MATLAB™[26] interactive software package was used to carry out most of the calculations in this thesis. All required procedures were encoded as MATLAB M-files,

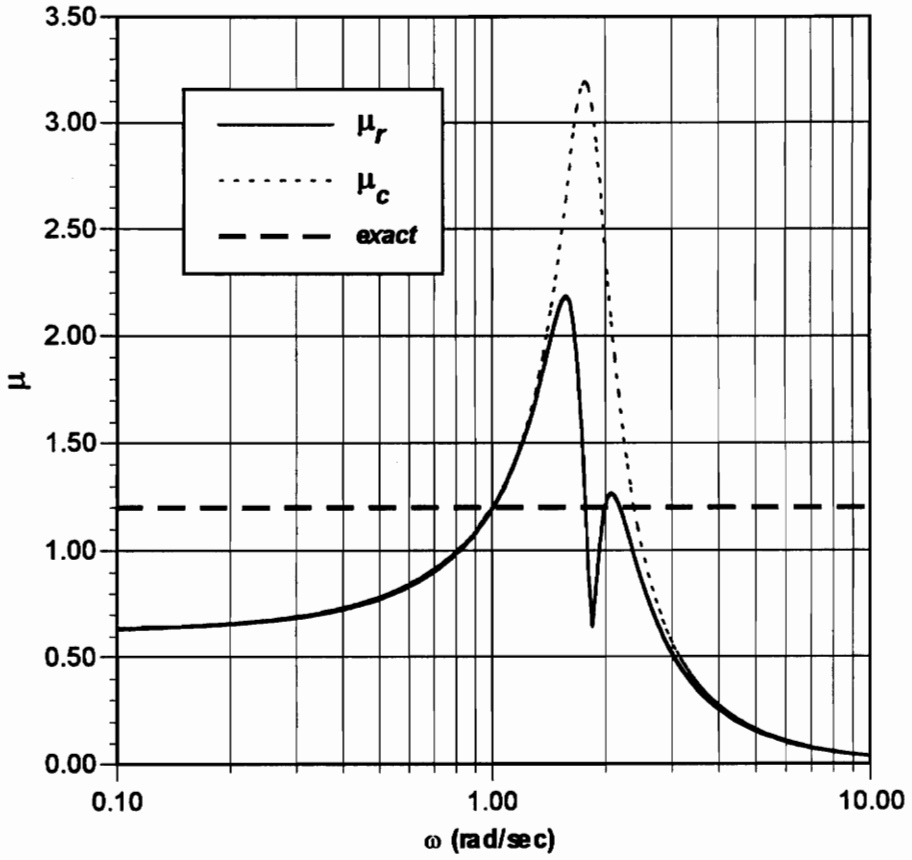

Figure 8. Departure resistance of example fourth-order model.

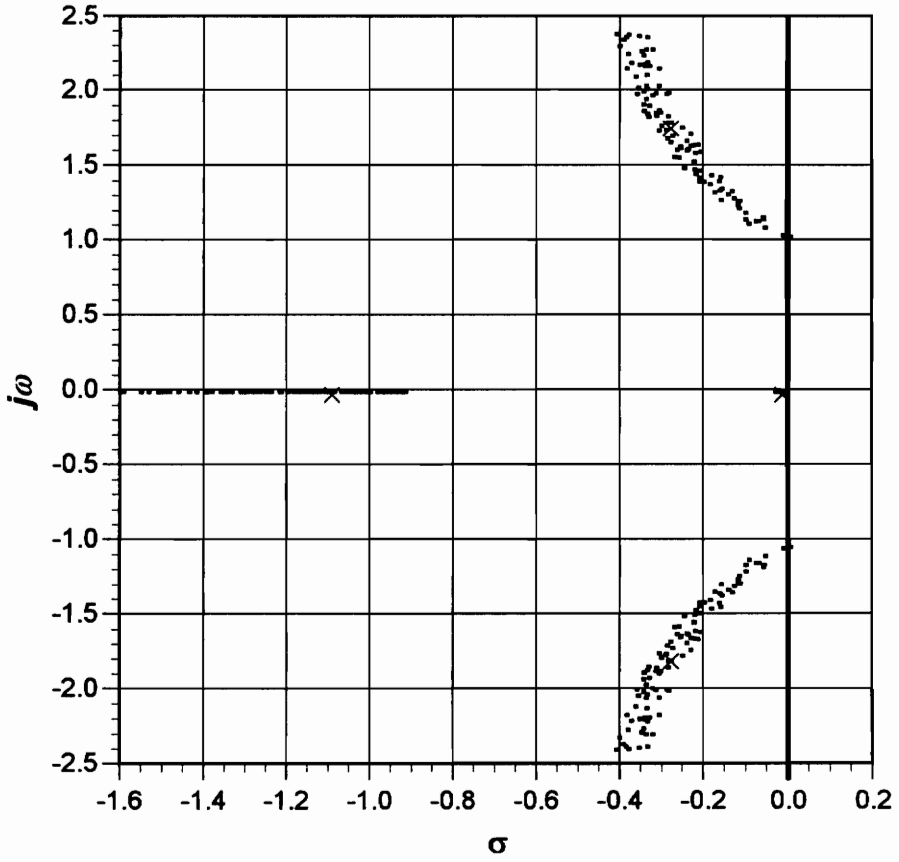

Figure 9. Eigenvalue scatter plot for example fourth-order model.

which are program-like script files used within MATLAB to automate frequently executed groups of commands. Important M-files are included with this thesis as an Appendix. These script files were used to assess the usefulness of DP_{SSV} in investigating aircraft departure resistance by analyzing aerodynamic data obtained from a full six degree-of-freedom, nonlinear aircraft simulation.

3.2.1. Aircraft Simulation

The model used in this study was one derived from existing nonlinear models of typical high-performance fighter-type aircraft. The simulation is a **G**eneric High-Performance **F**ighter **A**ircraft **N**onlinear **S**imulation, referenced by the acronym **FANGS** hereafter. This simulation is based primarily on the nonlinear aircraft model developed by Brumbaugh[27] for the AIAA Controls Design Challenge, the original FORTRAN source code for which was obtained from NASA Dryden. The simulation is not intended to be representative of any particular aircraft, but typifies the broad class of high-performance fighters. **FANGS** was used to produce all the data used in this research.

A trimming algorithm based on sequential quadratic programming is included in **FANGS**. This algorithm is a *generalized trim* routine; that is, it allows nonzero angular rates to be specified for the aircraft trim condition.[28] Though the vehicle is "instantaneously trimmed" at each point examined in this study, it is not necessarily in steady equilibrium, due to the presence in some configurations of roll, pitch, or yaw rate commands. The orientation of the aircraft can change due to these commanded angular rates, producing nonzero accelerations "instantly" after the trim point. The controls used to trim the aircraft are elevator (δ_h), rudder (δ_r), aileron (δ_a), bank angle (ϕ), throttle (π), and velocity (V). The constraints placed on these controls are listed in Table 1. The controls were adjusted by the trimming algorithm such that the angular rates p, q, and r remained at their commanded trim values, but their derivatives were reduced to zero. The cost function used by the trimming algorithm is

$$f = \dot{V}^2 + \dot{h}^2 + 10 * \left(\dot{p}^2 + \dot{q}^2 + \dot{r}^2\right) + 100 * \left(\dot{\alpha}^2 + \dot{\beta}^2\right). \tag{3.22}$$

TABLE 1. Trim constraints for **FANGS** simulation.

CONTROL	MINIMUM	MAXIMUM	UNITS	LIMIT
elevator	-25	15	degrees	FANGS
rudder	-20	20	degrees	FANGS
aileron	-30	30	degrees	FANGS
bank angle	-60	60	degrees	arbitrary
throttle	30	120	degrees	FANGS
velocity	300	1,000	feet/second	subsonic

The trim configurations investigated in this research are listed in Table 2. Each trim point was examined to ensure that the angular accelerations had indeed been reducible to near zero. Though the cost function given in equation (3.22) was always minimized by the trimming algorithm, it was not always reduced to zero, because the aircraft was unable to attain trim at many tested flight conditions due to a lack of control authority (the control surfaces were hitting their stops). If any angular acceleration had a magnitude greater than 0.1 degrees/second, the associated flight condition was discarded as outside the trimmable region. Figures 10 through 12 depict the trimmable regions for the **FANGS** simulation for the cases examined in this study.

A linear model extractor was added to the simulation to generate an A matrix for each trim point. The Jacobian matrix of the nonlinear simulation with respect to its states was determined at each trim point and stored along with information about the configuration of the aircraft.[29] It was assumed for this research that any point at which the aircraft could not be trimmed would not yield a meaningful linear model; therefore, only flight conditions inside the trimmable regions plotted in Figures 10 through 12 were considered in this research.

Finally, the aerodynamic characteristics of the simulated aircraft were altered slightly to approximate more closely the properties of interest in this type of vehicle. This modification involved simply reducing the effective dihedral by a multiplicative factor in order to bring the zero-sideslip values of the aerodynamic derivatives into reasonable agreement with those published for typical fighter aircraft.[13]

3.2.2. Case Study Procedures

Three sets of trim points were produced as described above, called Configurations I through III. Each set was then analyzed in several ways.

First, an eigenvalue analysis was performed on the extracted linear models to determine the stability of the aircraft model at each trim point. Several modes of low angular frequency were unstable throughout the flight envelope of the aircraft. Therefore, complex eigenvalues whose angular frequency was less than 0.1 radians/second were

TABLE 2. FANGS simulation trim configurations examined.

CONFIGURATION	*p* (deg/sec)	*q* (deg/sec)	*r* (deg/sec)	*h* (ft)
I	0	0	0	20,000
II	10	0	0	20,000
III	0	0	5	20,000

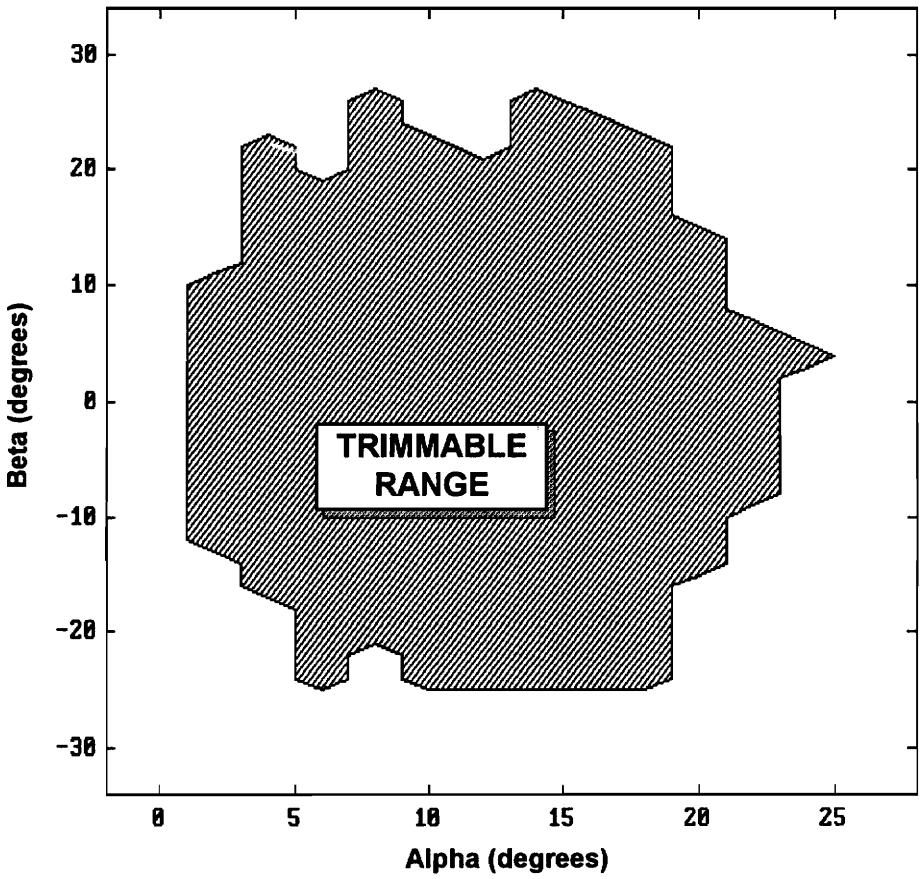

Figure 10. Trimmable range of **FANGS** simulation, Configuration I.

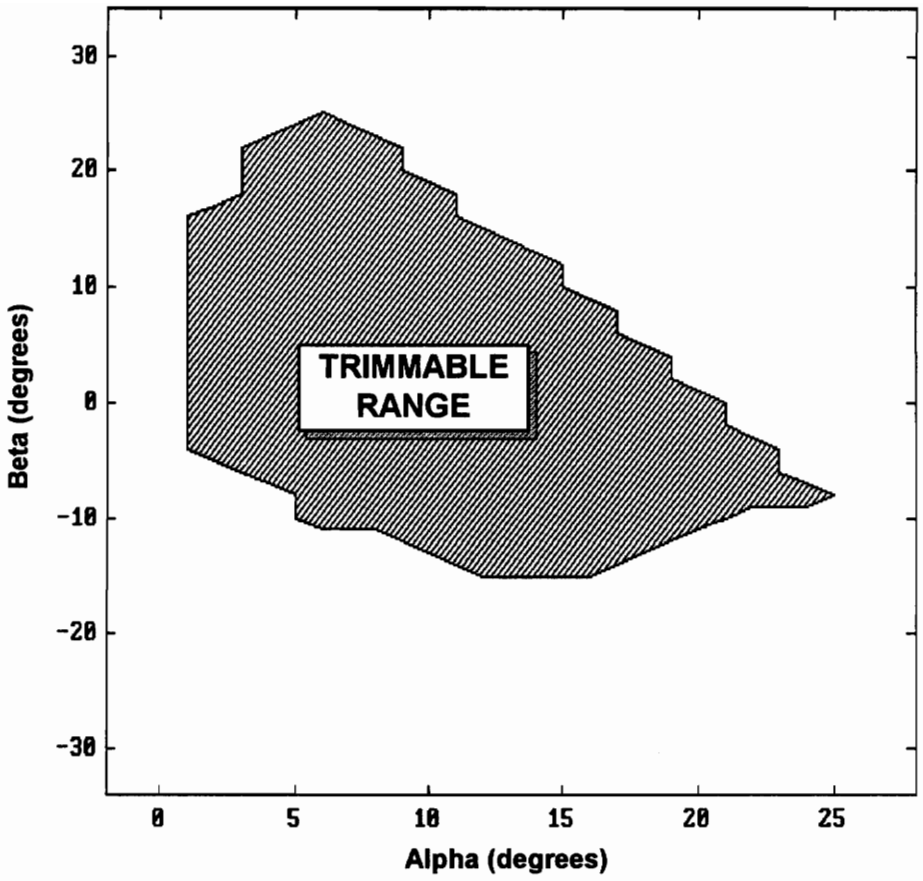

Figure 11. Trimmable range of **FANGS** simulation, Configuration II.

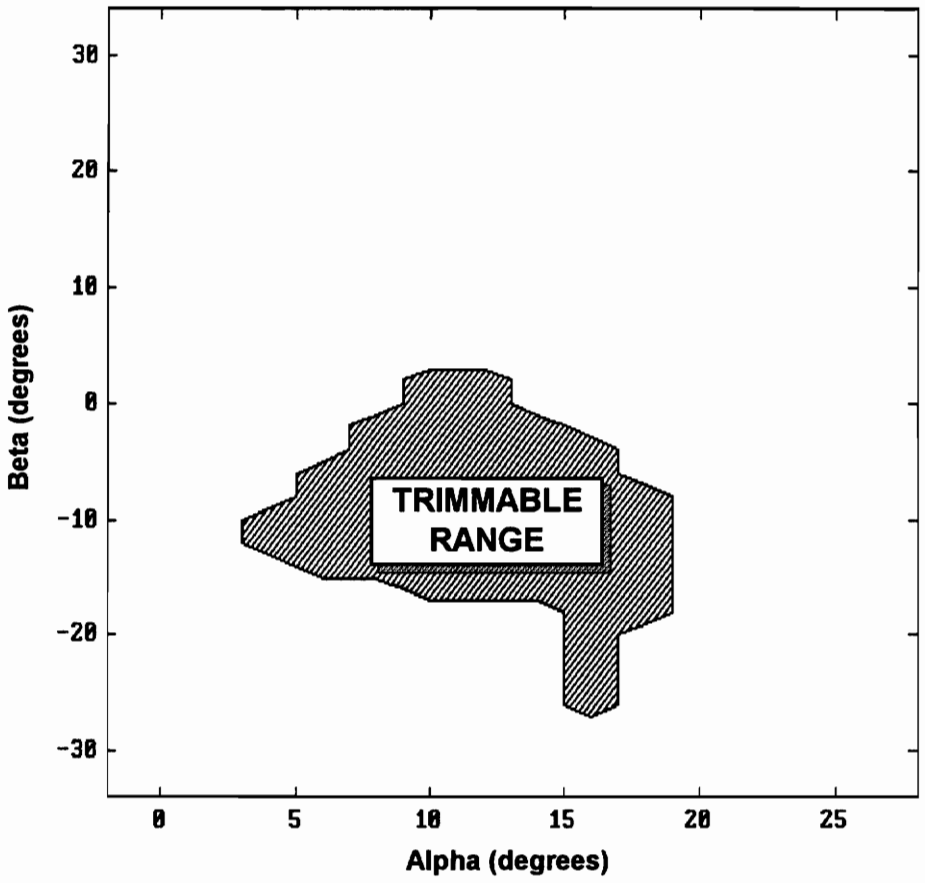

Figure 12. Trimmable range of **FANGS** simulation, Configuration III.

discarded. Additionally, any real eigenvalue with a value less than 0.25 was ignored. The remaining eigenvalues were used to assess the stability of the aircraft.

The traditional departure resistance parameter $C_{n_{\beta_{DYN}}}$ was then used to investigate the characteristics of the aircraft. $C_{n_{\beta_{DYN}}}$ was chosen for comparison purposes because it is probably the most widely used of the traditional departure resistance metrics.[13] This parameter was calculated at each trim point, and the customary criterion was applied; that is, the aircraft was assumed to be "departure free" for $C_{n_{\beta_{DYN}}} > 0$, and "departure prone" for $C_{n_{\beta_{DYN}}} \leq 0$. The metric was calculated by extracting values from the linearized A matrix at each trim point according to the following derivation. The lateral-directional small perturbation equations of motion include[30]

$$\dot{p} - R_x\dot{r} = L_\beta\beta + L_p p + L_r r + L_\delta\delta \tag{3.24a}$$

and

$$\dot{r} - R_z\dot{p} = N_\beta\beta + N_p p + N_r r + N_\delta\delta, \tag{3.24b}$$

where

$$R_x = \frac{I_{xz}}{I_{xx}},\ R_z = \frac{I_{xz}}{I_{zz}}. \tag{3.25}$$

Solving for $\dot{p}$ and $\dot{r}$ yields the following equations:

$$\begin{aligned}\dot{p} &= \frac{L_\beta + R_x N_\beta}{1 - R_x R_z}\beta + \frac{L_p + R_x N_p}{1 - R_x R_z}p + \frac{L_r + R_x N_r}{1 - R_x R_z}r + \frac{L_\delta + R_x N_\delta}{1 - R_x R_z}\delta, \\ \dot{r} &= \frac{N_\beta + R_z L_\beta}{1 - R_x R_z}\beta + \frac{N_p + R_z L_p}{1 - R_x R_z}p + \frac{N_r + R_z L_r}{1 - R_x R_z}r + \frac{N_\delta + R_z L_\delta}{1 - R_x R_z}\delta.\end{aligned} \tag{3.26}$$

Therefore,

$$\frac{\partial\dot{p}}{\partial\beta} = \frac{L_\beta + R_x N_\beta}{1 - R_x R_z} \tag{3.27a}$$

and

$$\frac{\partial\dot{r}}{\partial\beta} = \frac{N_\beta + R_z L_\beta}{1 - R_x R_z}. \tag{3.27b}$$

Solving these equations for N_β and L_β gives the following result:

$$\begin{aligned}L_\beta &= \left(\frac{1 - R_x R_z}{R_z - R_x^{-1}}\right)\frac{\partial\dot{r}}{\partial\beta} + \frac{\partial\dot{p}}{\partial\beta}, \\ N_\beta &= \left(\frac{1 - R_x R_z}{R_x - R_z^{-1}}\right)\frac{\partial\dot{p}}{\partial\beta} + \frac{\partial\dot{r}}{\partial\beta}.\end{aligned} \tag{3.28}$$

The quantities $\frac{\partial \dot{p}}{\partial \beta}$ and $\frac{\partial \dot{r}}{\partial \beta}$ are taken from the aircraft's A matrix; they are elements $A_{1,6}$ and $A_{3,6}$, respectively. Then using

$$C_{n_\beta} = \frac{I_{zz}}{\bar{q}Sb} N_\beta, \qquad C_{l_\beta} = \frac{I_{xx}}{\bar{q}Sb} L_\beta, \tag{3.29}$$

a value for $C_{n_{\beta_{DYN}}}$ can be obtained as per equation (2.5).

Finally, the new departure resistance criterion DP_{SSV} was used to analyze the aircraft model. For this investigation of departure resistance, uncertainty was considered in the A matrix elements $\frac{\partial \dot{p}}{\partial \beta}$ and $\frac{\partial \dot{r}}{\partial \beta}$ because of their close relationship to $C_{n_{\beta_{DYN}}}$. The states of the linearized **FANGS** state space model are

$$x^T = \begin{bmatrix} p & q & r & V & \alpha & \beta & \theta & h & T_L & T_R \end{bmatrix}. \tag{3.30}$$

Thus, the matrices E and F were chosen to be

$$E = \begin{bmatrix} \frac{\partial \dot{p}}{\partial \beta}_0 & 0 \\ 0 & 0 \\ 0 & \frac{\partial \dot{r}}{\partial \beta}_0 \\ 0 & 0 \\ 0 & 0 \\ 0 & 0 \\ 0 & 0 \\ 0 & 0 \\ 0 & 0 \\ 0 & 0 \end{bmatrix} \tag{3.31}$$

and

$$F = \begin{bmatrix} 0 & 0 & 0 & 0 & 0 & 1 & 0 & 0 & 0 & 0 \\ 0 & 0 & 0 & 0 & 0 & 1 & 0 & 0 & 0 & 0 \end{bmatrix}, \tag{3.32}$$

where $\frac{\partial \dot{p}}{\partial \beta}_0$ and $\frac{\partial \dot{r}}{\partial \beta}_0$ represent the nominal values of these derivatives, *i.e.*, the values in the A matrix obtained by linearizing the aircraft simulation. These values are included in the E

matrix to nondimensionalize the results. Using these definitions for E and F produces a two-by-two Δ (uncertainty) matrix defined by

$$\Delta = \begin{bmatrix} \dfrac{\delta\left(\frac{\partial \dot{p}}{\partial \beta}\right)}{\frac{\partial \dot{p}}{\partial \beta}_0} & 0 \\ 0 & \dfrac{\delta\left(\frac{\partial \dot{r}}{\partial \beta}\right)}{\frac{\partial \dot{r}}{\partial \beta}_0} \end{bmatrix}, \tag{3.33}$$

where $\delta(\cdot)$ represents the uncertainty in the specified aerodynamic derivative. Thus, the diagonal elements of Δ indicate the percentage uncertainty in the derivatives of interest. Since DP_{SSV} represents the size of Δ in terms of its spectral or 2-norm, it quantifies for this case an upper bound on the uncertainty in the aerodynamic derivatives such that

$$DP_{SSV} \geq \max\left\{ \left| \frac{\delta\left(\frac{\partial \dot{p}}{\partial \beta}\right)}{\frac{\partial \dot{p}}{\partial \beta}_0} \right|, \left| \frac{\delta\left(\frac{\partial \dot{r}}{\partial \beta}\right)}{\frac{\partial \dot{p}}{\partial \beta}_0} \right| \right\} \tag{3.34}$$

must be satisfied. Thus, DP_{SSV} essentially defines an upper limit on the percentage change allowed simultaneously in both aerodynamic derivatives without inducing instability.

For the cases examined in this research, Δ is always a two-by-two matrix, so M is also two-by-two. In such instances, Osborne's method can be solved exactly to find the scaling matrix D to minimize $\|DMD^{-1}\|_F$ as required by equation (3.10), and no iteration for the purpose of minimization is required. Letting

$$D = \begin{bmatrix} d_1 & 0 \\ 0 & d_2 \end{bmatrix} = d_1 \begin{bmatrix} 1 & 0 \\ 0 & \frac{d_2}{d_1} \end{bmatrix}, \tag{3.35}$$

gives

$$\begin{aligned} \|DMD^{-1}\|_F &= \left\| d_1 \begin{bmatrix} 1 & 0 \\ 0 & \frac{d_2}{d_1} \end{bmatrix} M \frac{1}{d_1} \begin{bmatrix} 1 & 0 \\ 0 & \frac{d_1}{d_2} \end{bmatrix} \right\|_F \\ &= \left\| \begin{bmatrix} 1 & 0 \\ 0 & d \end{bmatrix} M \begin{bmatrix} 1 & 0 \\ 0 & \frac{1}{d} \end{bmatrix} \right\|_F \end{aligned} \tag{3.36}$$

where d has been defined as $\frac{d_2}{d_1}$. Thus only one degree of freedom exists in finding the scaling matrix. Defining

$$M = \begin{bmatrix} m_{11} & m_{12} \\ m_{21} & m_{22} \end{bmatrix}, \tag{3.37}$$

it can be shown that the d required to minimize equation (3.36) is

$$d = \left(\frac{m_{12}^* \, m_{12}}{m_{21}^* \, m_{21}} \right)^{\frac{1}{4}}. \tag{3.38}$$

Equation (3.38) was used to find the appropriate scaling matrix for all data examined.

To find the minimum with respect to angular frequency as indicated in equation (3.12), a fairly coarse frequency sweep was performed over the range of interest, and then a golden section search was used to find ω_{SSV} to a tolerance of 0.0005 radians/second.[31] The MATLAB M-file used for this search, DPSRCH.M, is reproduced in the Appendix.

4. Results and Discussion

4.1. Case Study Results

The operations described in the Procedures section above were carried out on the three sets of data produced for this research, Configurations I through III. The results of each analysis are described below.

4.1.1. Configuration I — All Angular Rates Zero

Figure 13 shows the stable and unstable regions of the trimmable envelope for Configuration I as determined by examining the eigenvalues of the linearized A matrices. Figure 14 displays the departure resistance of the aircraft as predicted by $C_{n_{\beta_{DYN}}}$. It would be expected that the departure prone region of Figure 14 would be essentially the same as the unstable region of Figure 13, but this is not quite the case. The fact that a trim point is indicated as unstable in Figure 13 indicates that its instability is of sufficient speed to be classified as a departure condition, yet the $C_{n_{\beta_{DYN}}}$ analysis does not identify all these points as possibilities for a departure condition. Recall that Moul and Paulson expected the departure resistance predictions of $C_{n_{\beta_{DYN}}}$ to be somewhat conservative. However, this does not appear to be the case in Figure 14. Note that the areas of questionable agreement are located at sideslip angles near 20 degrees, flight conditions where $C_{n_{\beta_{DYN}}}$ might be expected to produce erroneous results.

Figure 15 is a three-dimensional plot of DP_{SSV}, showing its contours throughout the trimmable region. The interpretation of DP_{SSV} is that it indicates the maximum uncertainty allowed in the nominally stable aircraft before the system becomes unstable. Therefore, as points closer and closer to an unstable region are examined, the value of DP_{SSV} would be expected to drop, since a system can tolerate very little uncertainty if it is already near an instability boundary. When DP_{SSV} reaches a minimum and begins to rise again, an instability boundary has been crossed. Thus, the "valley" visible in Figure 15 can be interpreted as a boundary between departure free and departure prone regions for the

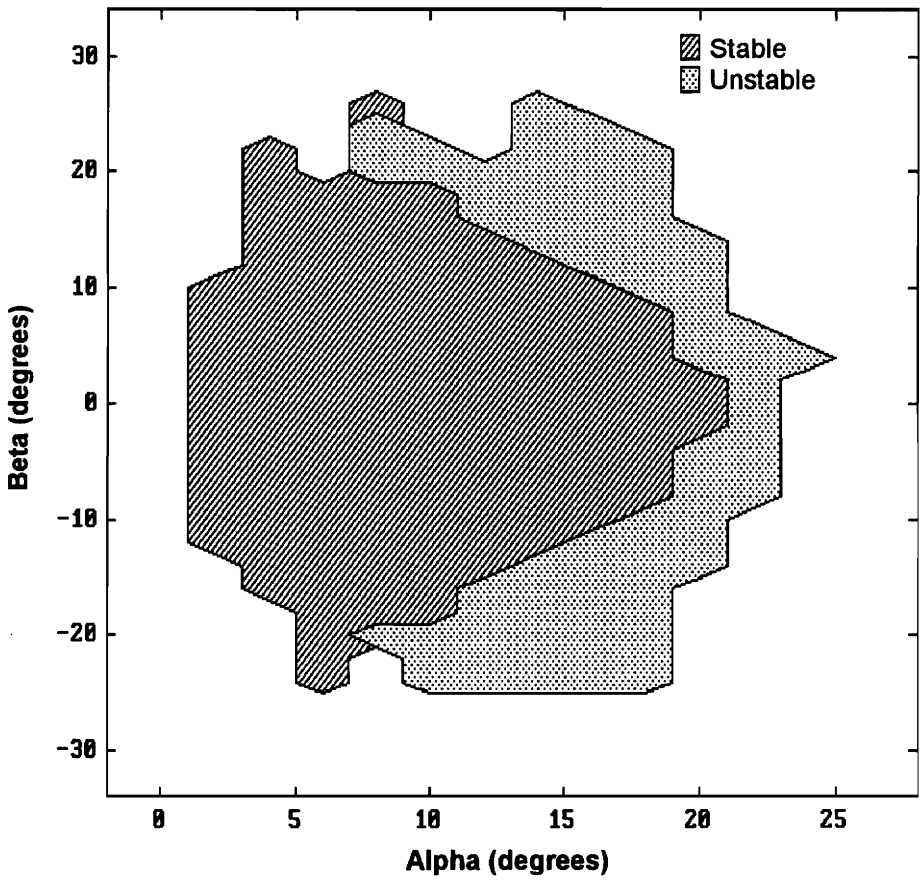

Figure 13. Stability of **FANGS** simulation, Configuration I, as indicated by eigenvalues of linearized models.

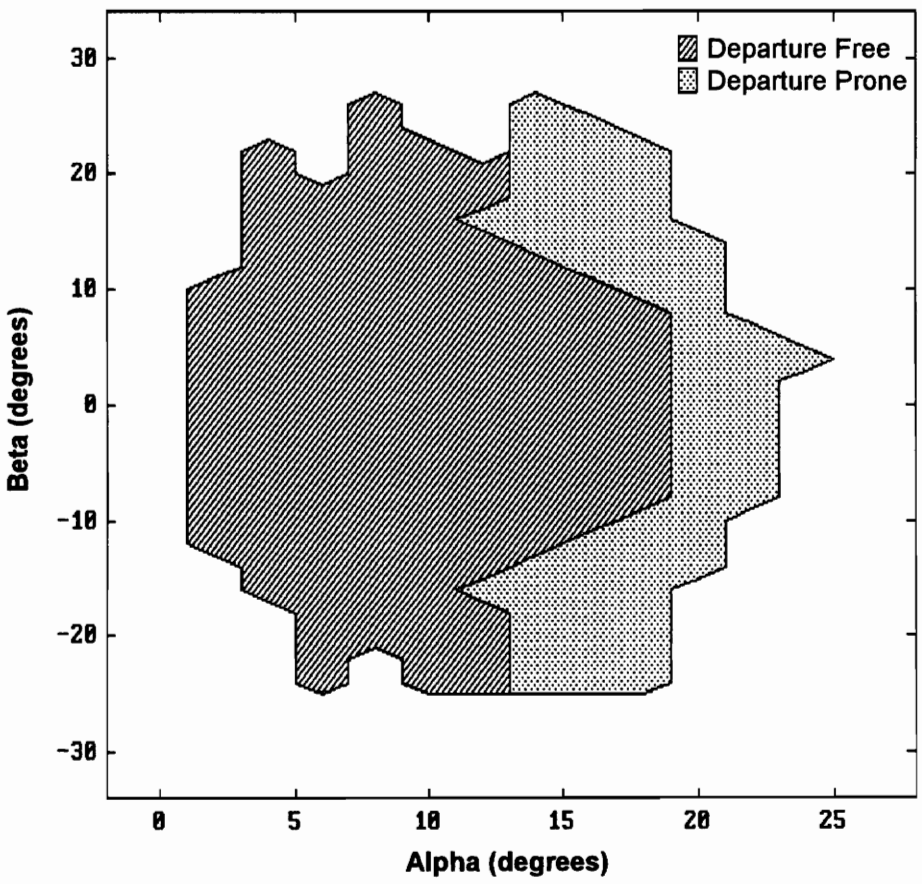

Figure 14. Departure resistance of **FANGS** simulation, Configuration I, as predicted by using $C_{n_{\beta_{DYN}}} > 0$ as departure resistance criterion.

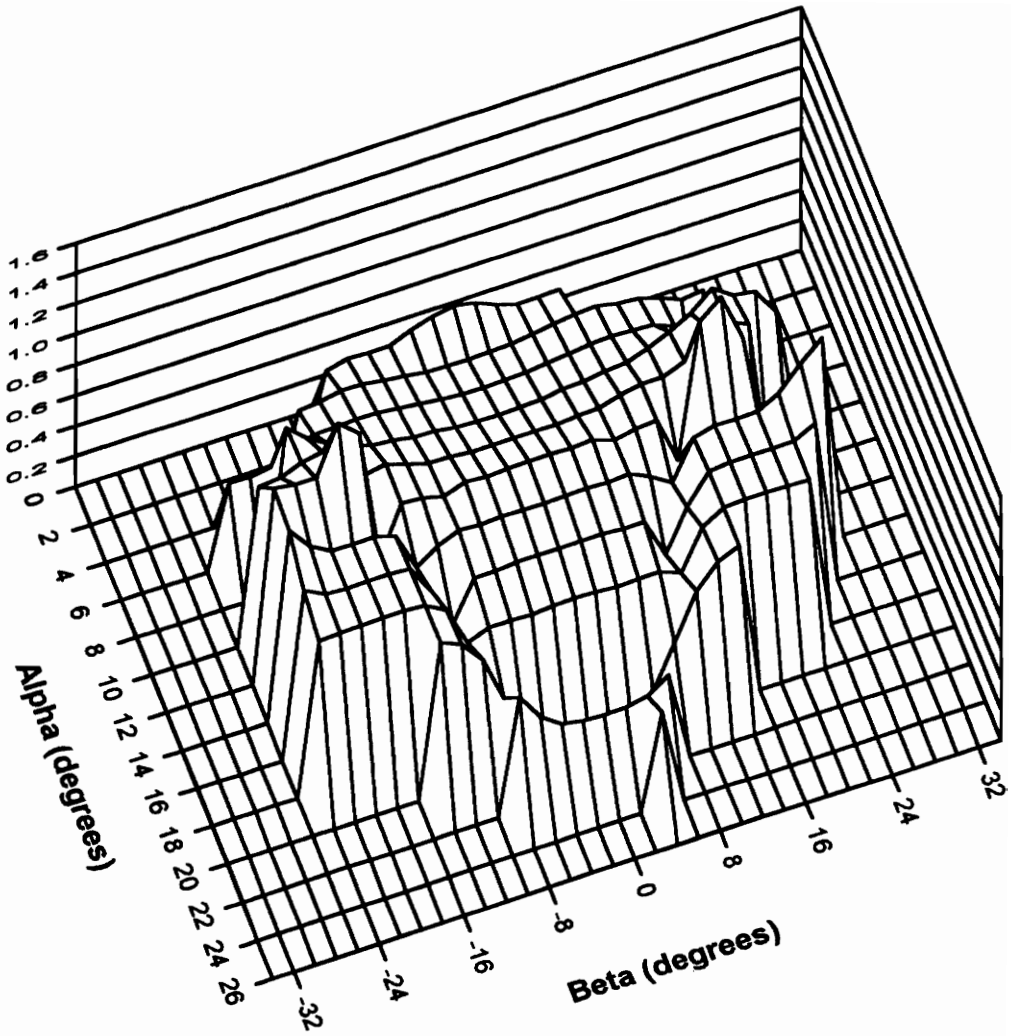

Figure 15. Three-dimensional plot of DP_{SSV} for Configuration I.

aircraft. Figure 16 is a contour plot of a portion of the data in Figure 15. Lighter shades represent smaller values for DP_{SSV}, while darker shades indicate larger values. The heavy line on the graph denotes the general location of the trough or valley, *i.e.*, the instability boundary. Note that the location of this valley is not as well defined by the data in some areas as it is in others; this is mainly due to the coarseness of the grid over which DP_{SSV} is calculated. Were the grid made arbitrarily fine, the boundary could be more easily identified. In addition, in some cases it is difficult to classify a point as "inside" or "outside" the boundary, a problem sometimes compounded by the presence of multiple valleys in the DP_{SSV} plot. Since the definition of μ requires that the nominal system be stable, no meaningful interpretation can be made for points lying outside the innermost boundary. Additional valleys beyond the first may represent stability boundaries for different modes, reentry into a stable region, or neither of these possibilities.

In addition to simply defining regions where the aircraft will be likely to experience departure, DP_{SSV} can be used to measure how close the aircraft is to such regions. By classifying areas close to the instability boundary where DP_{SSV} is less than some cutoff value as being marginal in their departure resistance, information is gained about which attitudes are "close" to a departure boundary. These marginal areas will not tolerate a large amount of uncertainty before being driven to a departure. Operating in marginal areas will not immediately cause the aircraft to undergo a departure, but the vehicle is nonetheless operating in a possibly dangerous area.

Figure 17 shows the departure characteristics of the aircraft as predicting by using these interpretations of DP_{SSV}. Regions "inside" the valley or instability boundary where $DP_{SSV} > 0.6$ are classified as departure free. Those areas inside the boundary where $DP_{SSV} \leq 0.6$ are labelled marginal. The remaining regions — those located outside the instability boundary — are termed departure prone. Note that the value 0.6 used here is arbitrary, but considered reasonable to indicate marginal departure resistance.

There is reasonably good agreement between the departure susceptibility predictions made by DP_{SSV} in Figure 17 and the stability map shown in Figure 13.

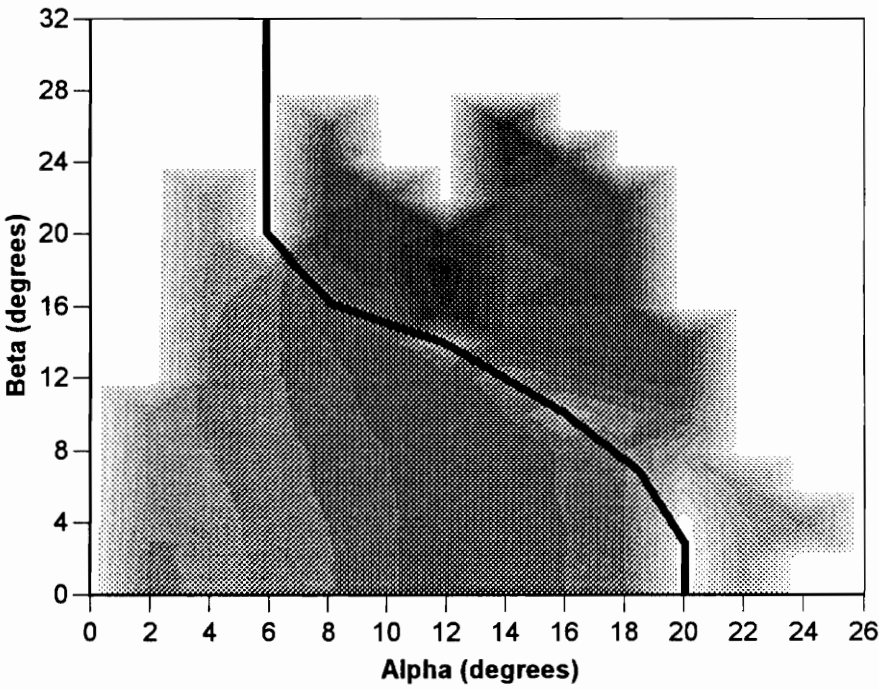

Figure 16. Contour plot of DP_{ssv} for Configuration I.

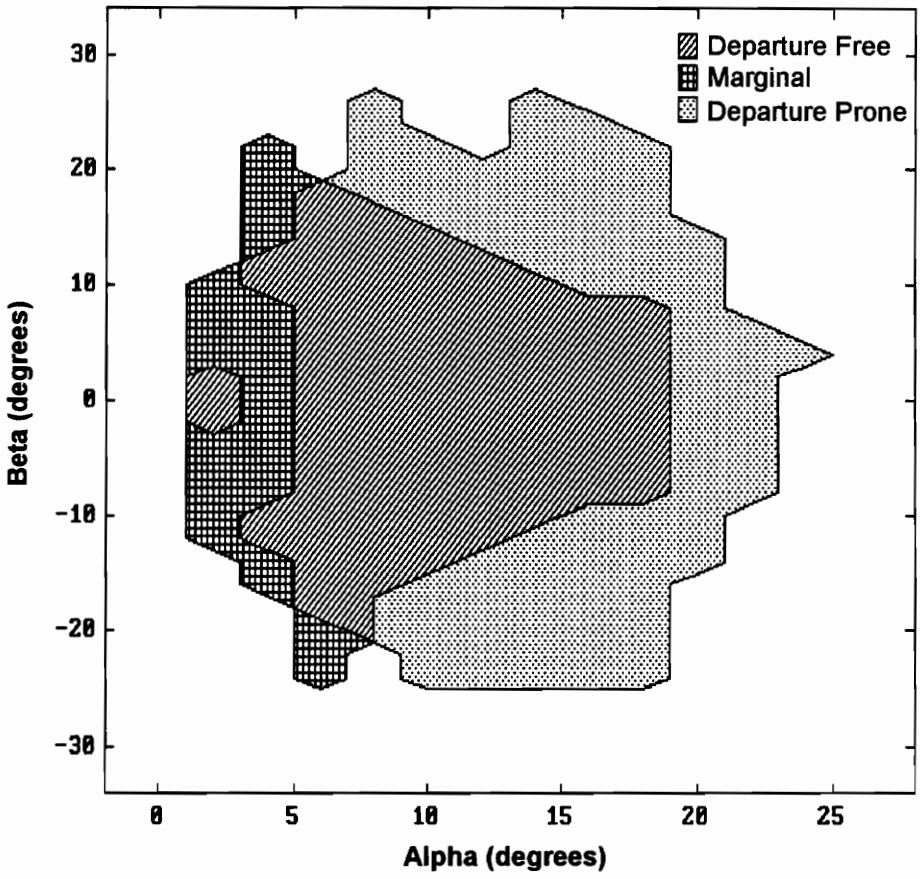

Figure 17. Departure resistance of **FANGS** simulation, Configuration I, as predicted by using DP_{SSV} as departure resistance criterion.

Essentially the entire area labelled as unstable in Figure 13 is identified as departure prone by the DP_{SSV} analysis. Since the new metric is conservative, it labels some additional points as unstable that are not so identified by eigenvalue analysis. Note that the predictions at large sideslip angle are quite good, in contrast to those of $C_{n_{\beta_{DYN}}}$.

The only areas identified as marginal in Figure 17 are located near the edge of the trimmable envelope. Identification of these areas illustrates an important advantage of the new metric — information gained from DP_{SSV} concerns not only the point at which the metric is calculated, but also points in the neighborhood. Since the value calculated for DP_{SSV} varies smoothly across α–β space, information about nearby points can be inferred from calculation of the metric at a given point. The marginal areas depicted in Figure 17 may be identifying unstable regions just beyond the trim envelope, where eigenvalue analysis was not performed.

Figure 18 represents a three-dimensional plot of T_{SSV}, the period of the closest unstable mode to each trim point. The "plateaus" visible at angles of attack from about 12 to 20 degrees indicate that the closest instability has a frequency of less than 0.1 radians/second, the smallest frequency examined.

4.1.2. Configuration II — Nonzero Roll Rate

Figure 19 displays the stable and unstable regions of the trimmable envelope of Configuration II as determined from an eigenvalue analysis of the linearized models of the bare airframe. Figure 20 shows the departure resistance of the aircraft as predicted by $C_{n_{\beta_{DYN}}}$. Note that the unstable areas at low sideslip angle are predicted well by this criterion, but there are a few small unstable areas for $\beta > 10$ degrees which are not reflected in the departure prone regions of Figure 20.

Figure 21 is a three-dimensional plot of DP_{SSV} for the entire trimmable region of Configuration II. By examining this figure, it can be seen that there is only a small area at high α that is located beyond an instability boundary. This result is reflected in the departure resistance plot of Figure 22. However, again applying the criterion of $DP_{SSV} < 60\%$, an additional area of marginal departure resistance is observed. Note that,

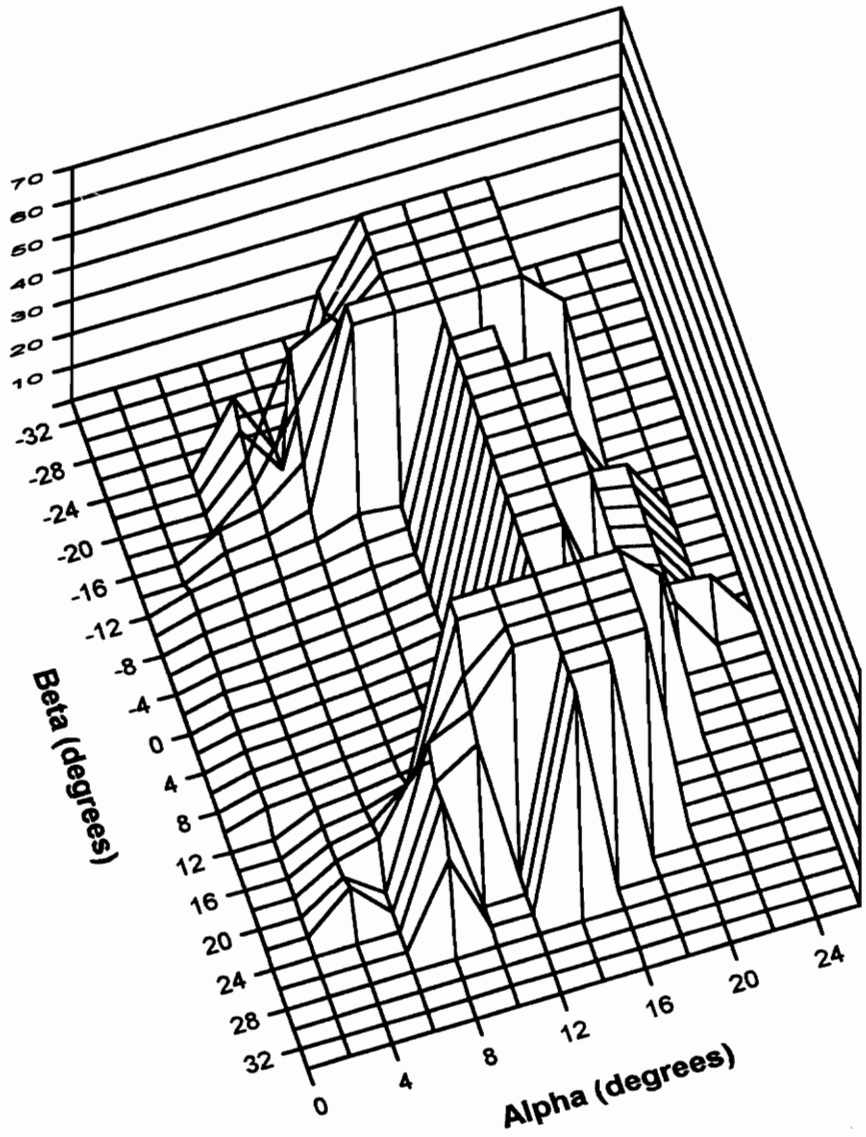

Figure 18. Three-dimensional plot of T_{SSV} for Configuration I.

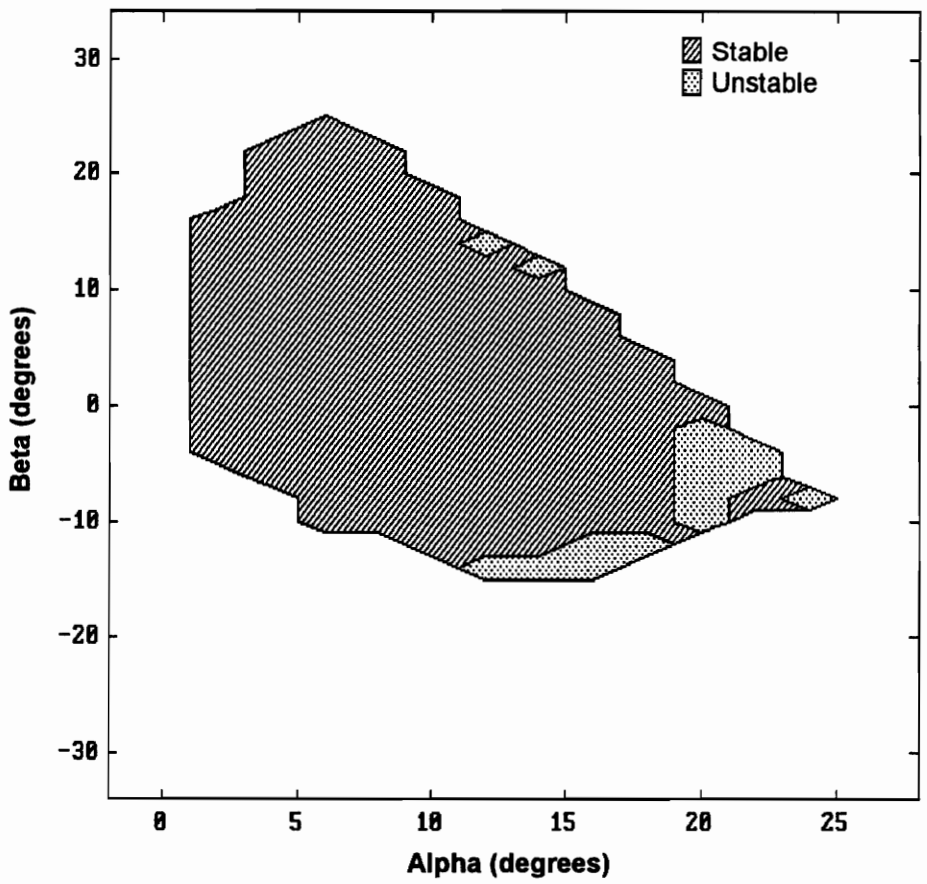

Figure 19. Stability of **FANGS** simulation, Configuration II, as indicated by eigenvalues of linearized models.

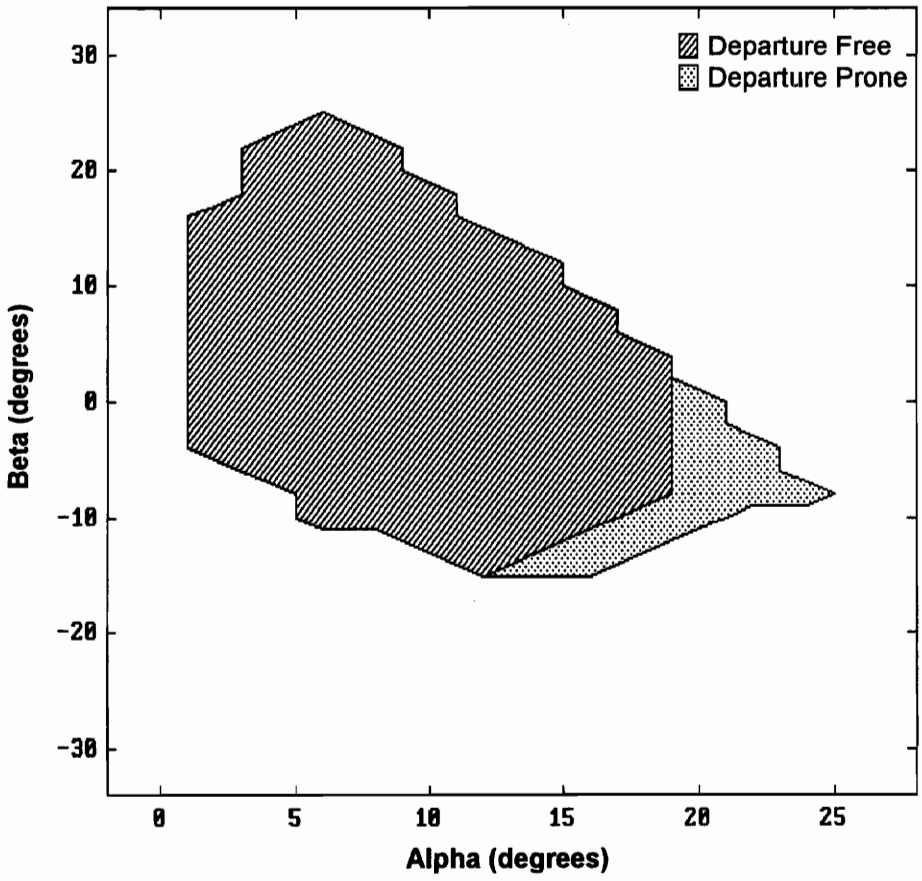

Figure 20. Departure resistance of **FANGS** simulation, Configuration II, as predicted by using $C_{n_{\beta_{DYN}}} > 0$ as departure resistance criterion.

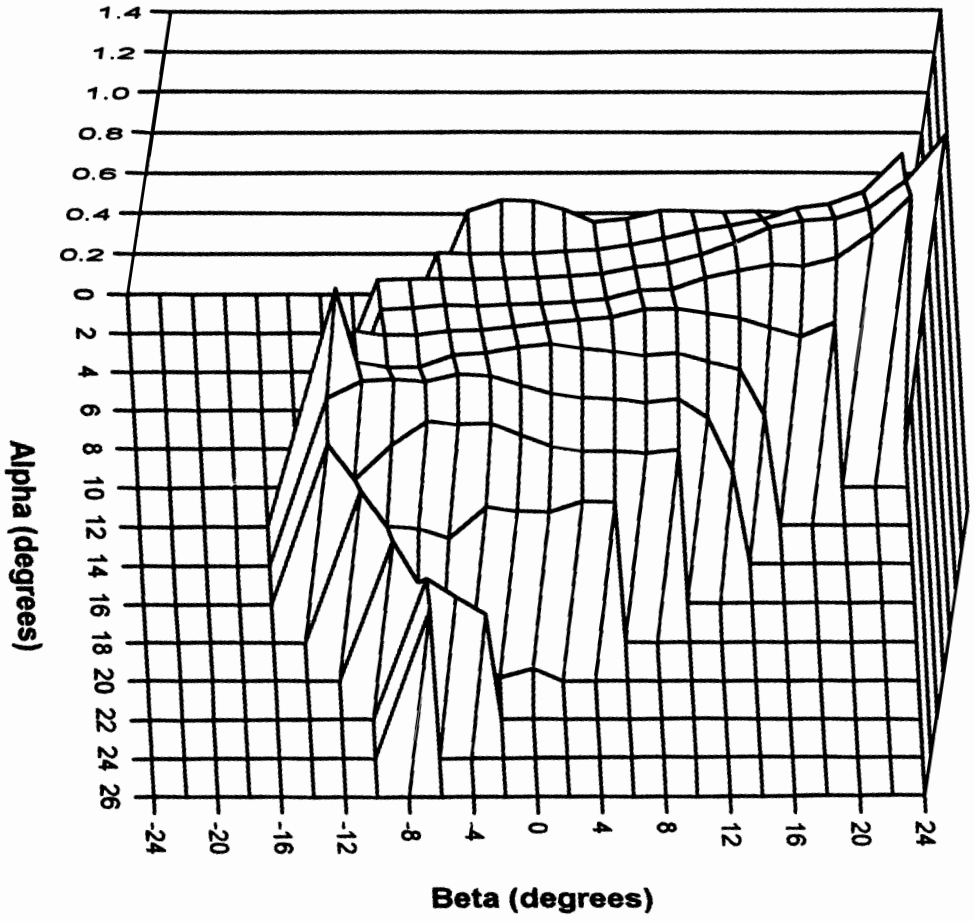

Figure 21. Three-dimensional plot of DP_{ssv} for Configuration II.

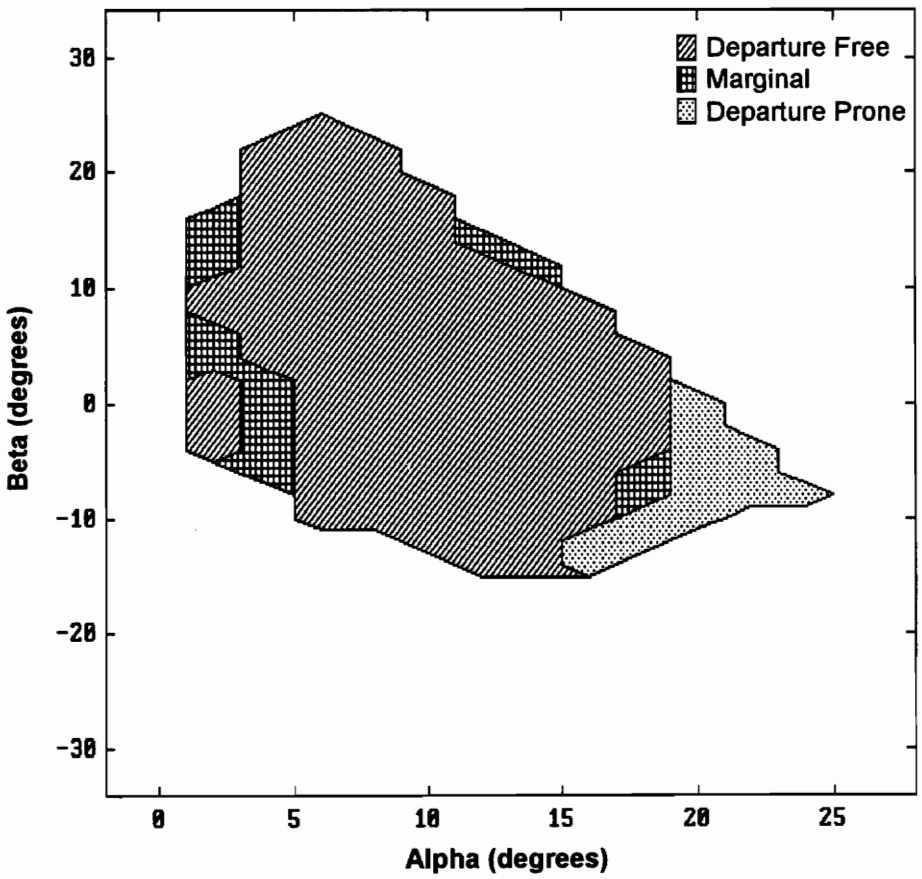

Figure 22. Departure resistance of **FANGS** simulation, Configuration II, as predicted by using DP_{SSV} as departure resistance criterion.

although the regions where $\beta > 10$ degrees classified as unstable in Figure 19 are not identified as unstable, they are included within the marginal area. Additional marginal regions are observed at low alpha, similar to the results obtained for Configuration I.

4.1.3. Configuration III — Nonzero Yaw Rate

Figure 23 shows the stable and unstable regions of the trimmable envelope for Configuration III. Note that most of the trimmable region is classified as unstable. Figure 24 displays departure resistance as indicated by analysis of $C_{n_{\beta_{DYN}}}$. The metric predicts a departure prone region at relatively high α and large β, but classifies most of the trimmable area as departure free.

Figure 25 displays a three-dimensional plot of DP_{SSV} for the trimmable region. Again a "valley" is clearly visible in this plot, representing an instability boundary. Figure 26 shows the departure resistance of the aircraft as predicted by DP_{SSV}. A larger unstable area is predicted than in Figure 24, which seems more representative of the true stability of the model given in Figure 23. However, though small portions of the trim envelope are identified as marginal, much of the area found to be unstable through eigenvalue analysis is indicated to be departure free by the DP_{SSV} analysis. The instabilities indicated are thus assumed to be related to some aerodynamic derivative other than the two chosen for this analysis ($\frac{\partial \dot{p}}{\partial \beta}$ and $\frac{\partial \dot{r}}{\partial \beta}$). This conclusion is supported by the fact that these instabilities were also not reflected in the analysis of $C_{n_{\beta_{DYN}}}$, which is based on the same derivatives. This result illustrates how the choice of quantities to be investigated affects the results provided by DP_{SSV}.

4.2. Summary and Discussion

The stability of the subject aircraft simulation was investigated through eigenvalue calculations. In addition, departure resistance prediction was performed using the traditional measure $C_{n_{\beta_{DYN}}}$ as well as the new metric DP_{SSV}. For Configuration I, where all angular rates were zero, good agreement was found between the predictions of DP_{SSV} and the eigenvalue analysis. It was discovered that $C_{n_{\beta_{DYN}}}$ did not predict instabilities in the

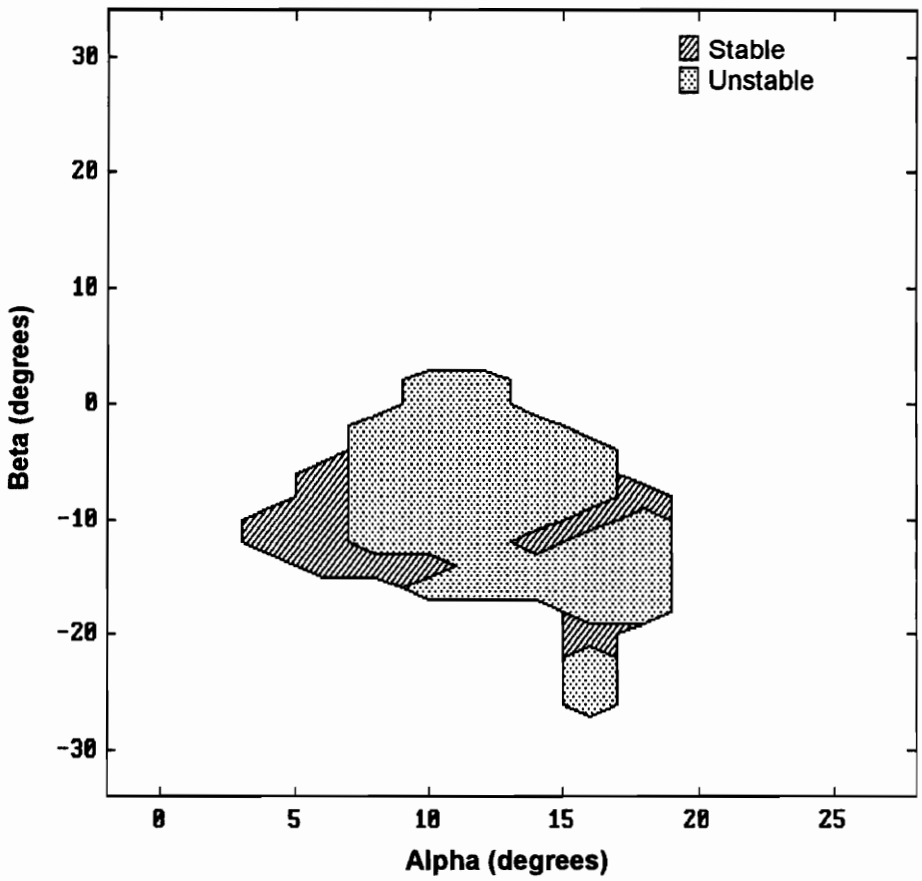

Figure 23. Stability of **FANGS** simulation, Configuration III, as indicated by eigenvalues of linearized models.

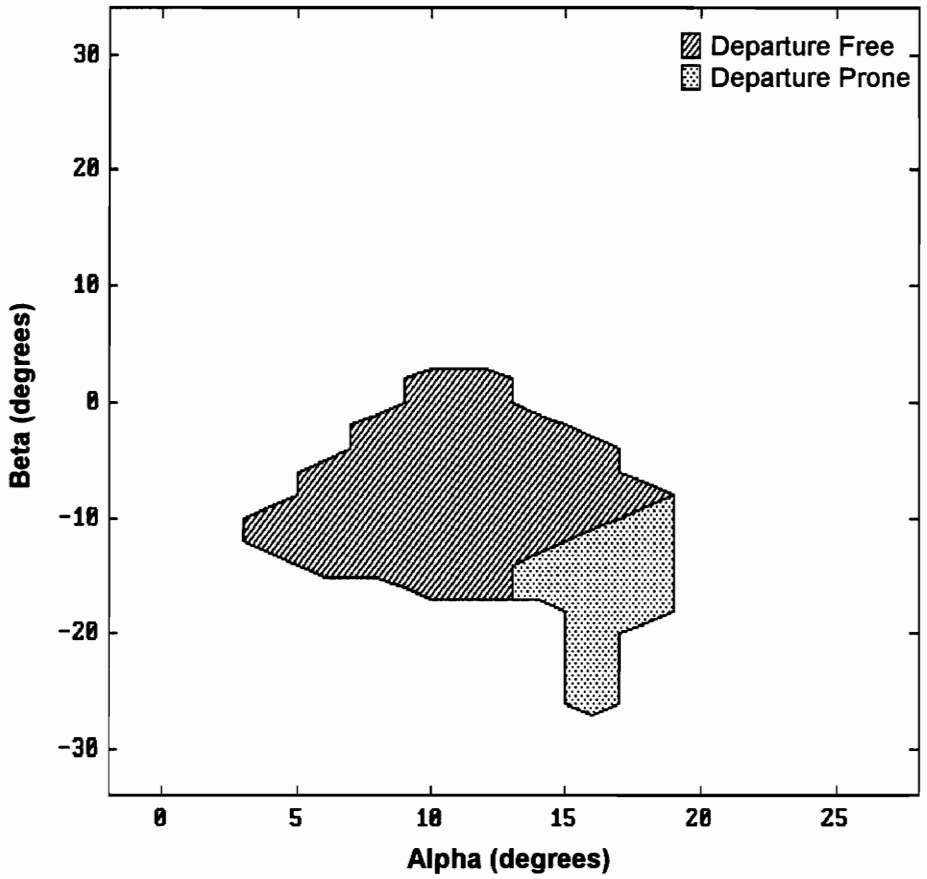

Figure 24. Departure resistance of **FANGS** simulation, Configuration III, as predicted by using $C_{n_{\beta_{DYN}}} > 0$ as departure resistance criterion.

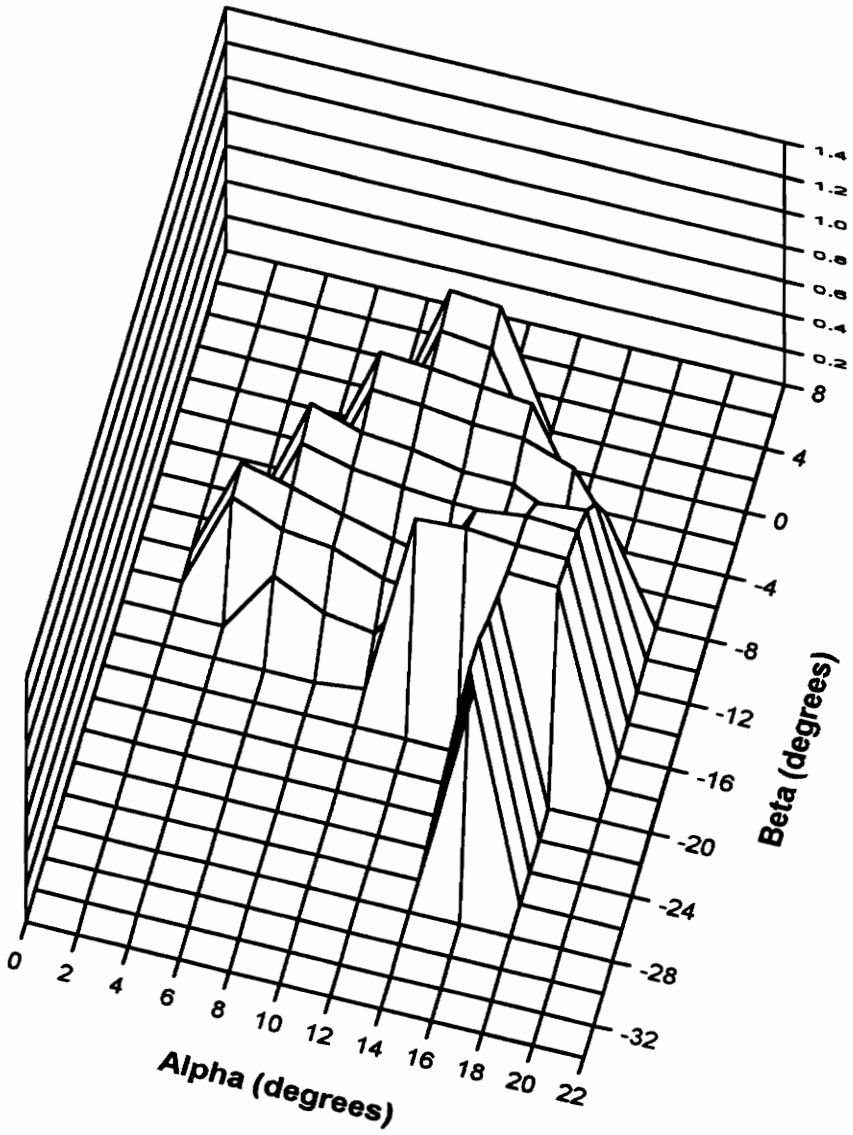

Figure 25. Three-dimensional plot of DP_{SSV} for Configuration III.

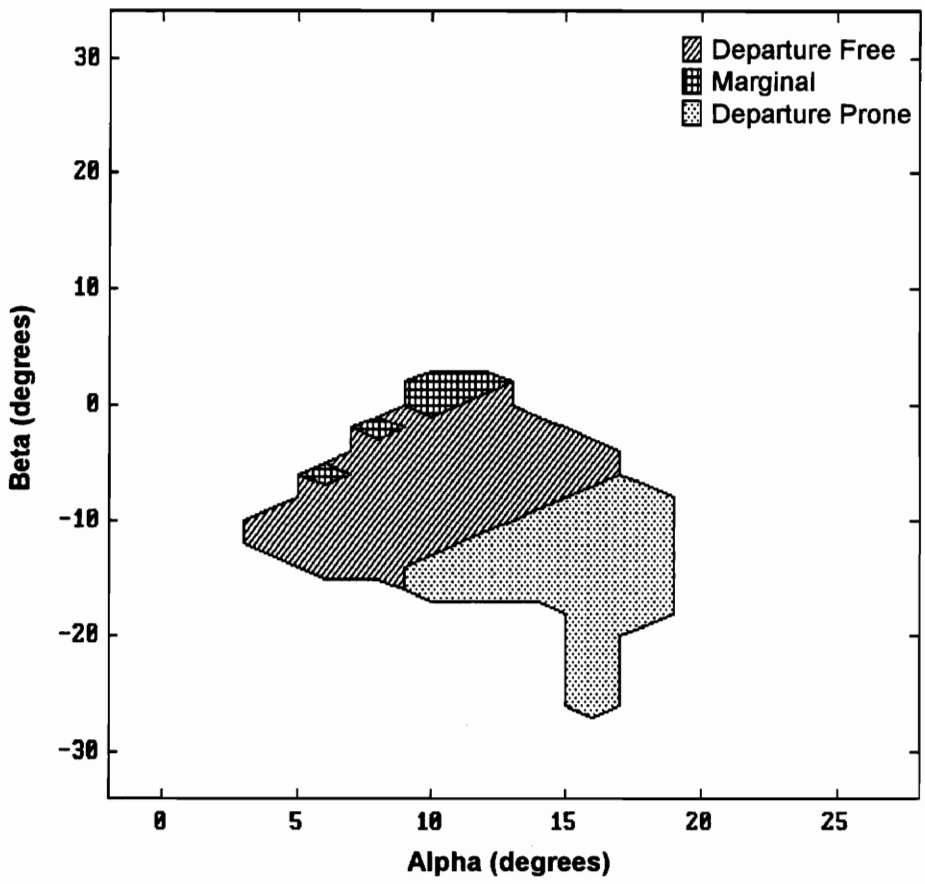

Figure 26. Departure resistance of **FANGS** simulation, Configuration III, as predicted by using DP_{SSV} as departure resistance criterion.

model well at large sideslip angles, while DP_{SSV} displayed good behavior in such regions. Areas of marginal departure resistance were identified from the DP_{SSV} results. It was also shown that calculation of DP_{SSV} provides information about the period of the nearest unstable mode.

For Configuration II, in which roll rate was nonzero, reasonably good correlation was observed between the results for DP_{SSV} and the eigenvalue stability map. Some areas identified as unstable by eigenvalue analysis were considered departure free by $C_{n_{\beta_{DYN}}}$, but were classified as marginal through DP_{SSV} calculations.

The results for DP_{SSV} and $C_{n_{\beta_{DYN}}}$ agreed well for Configuration III, in which yaw rate was nonzero. However, the eigenvalue analysis identified a large unstable area which was not predicted by either departure resistance metric. It was postulated that this unstable area was related to aerodynamic derivatives other than those used in the calculation of $C_{n_{\beta_{DYN}}}$ and DP_{SSV}.

Several observations can be made based on these results. Most importantly, DP_{SSV} has been shown to be a valid departure resistance metric. Departure susceptibility prediction performed using DP_{SSV} appears to be always at least as accurate as that provided by $C_{n_{\beta_{DYN}}}$, and in some cases the new metric gives better results.

In using DP_{SSV} for departure resistance analysis, a region can be defined where the aircraft is considered "close" to an instability boundary. Calculation of DP_{SSV} at a point produces data that reflect conditions not only at that point, but also throughout the neighborhood about that point. Thus information is obtained about nearby departure resistance characteristics, as was shown in the analyses for all three investigated configurations.

Though the new metric is generally conservative, some flight conditions at which the aircraft is unstable may not necessarily be identified as such by DP_{SSV}, depending on which elements of the model's A matrix are used in the calculation. This behavior was demonstrated by the analysis conducted for Configuration III.

5. Conclusions

Several interesting conclusions can be drawn from this research. It was shown that the structured singular value can be a useful indicator of the departure resistance of an aircraft at a given flight condition. This assertion was supported through calculation and interpretation of a new departure resistance parameter, DP_{SSV}, and through comparison of its predictions with those obtained by eigenvalue stability analysis and calculation of the traditional departure resistance metric $C_{n_{\beta_{DYN}}}$. The advantages gained through the use of the new parameter are numerous.

(a) The bare airframe eigenvalues need not be calculated to determine aircraft departure resistance and stability.

(b) The nonlinearities and modal coupling inherent in the aircraft are taken fully into account, with the model only linearized locally about the flight condition of interest.

(c) Control systems, nonstandard controllers, and many other effects can be easily included in the departure resistance calculation, rather than being limited to simply investigating the characteristics of the airframe alone.

(d) At any point, the aircraft's nearness to an instability, rather than simply its departure tendency, can be easily determined. Areas of "marginal" departure resistance can be identified.

Nevertheless, there are some caveats regarding the use of DP_{SSV}.

(a) DP_{SSV} does not have a meaningful interpretation for a nominally unstable system.

(b) The results obtained for departure resistance are usually somewhat conservative.

Further study is required to determine the effectiveness of DP_{SSV} in predicting departure resistance in other cases. For example, work might be done in actually calculating DP_{SSV} for a complete aircraft, including control systems, actuators, sensors,

etc. Research could also be performed on more accurate or simpler ways to calculate DP_{SSV} or a similar parameter, and on more effective interpretation of the results thus obtained.

Comparisons could be made between the results obtained for DP_{SSV} and nonlinear simulation trajectories. For example, time histories could be produced for both the nominal flight condition and the nominal condition perturbed by Δ, to provide additional insight into the interpretation of the departure parameter. Comparison with actual flight data would be instructive as well.

Applications of DP_{SSV} to the design of control systems could be investigated. The goal would be to use this metric directly in the design process to maximize departure resistance across the flight envelope. Strategies for balancing performance vs. departure resistance could be developed and applied to modern aircraft.

The most immediate opportunity for extended research is further investigation as to which elements or combinations of elements from the A matrix provide the best indication of departure resistance. The A matrix elements used for this research were those from which $C_{n_{\beta_{DYN}}}$ is calculated and were therefore assumed to be reasonably good indicators of departure characteristics, but it would be of interest to examine the use of other aerodynamic derivatives in the DP_{SSV} metric.

6. References

[1] Scott, W.B., "NASA Adds to Understanding of High Angle of Attack Regime," *Aviation Week & Space Technology,* v. 130, no. 21 (May 22, 1989), pp. 36-42.

[2] Dornheim, M.A., "X-31 Flight Tests to Explore Combat Agility to Seventy Degrees AOA," *Aviation Week & Space Technology,* v. 134, no. 10 (March 11, 1991), pp. 38-41.

[3] Henderson, B.W., "Dryden Completes First Flights of F/A-18 HARV with Thrust Vectoring," *Aviation Week & Space Technology,* v. 135, no. 4 (July 29, 1991), p. 25.

[4] Johnston, D.E., and Hogge, J.R., "The Effect of Non-Symmetric Flight on Aircraft High Angle of Attack Handling Qualities and Departure Characteristics," AIAA Paper no. 74-792, AIAA Mechanics and Control of Flight Conference, Anaheim, CA (August 5-9, 1974).

[5] Seltzer, R.M., and Rhodeside, G.R., "Fundamentals and Methods of High Angle-of-Attack Flying Qualities Research," Report No. NADC-88020-60, Naval Air Development Center, Warminster, PA (January 1988).

[6] "Military Standard — Flying Qualities of Piloted Aircraft," MIL-STD-1797 (March 1987).

[7] Bihrle, W., Jr., "Influence of the Static and Dynamic Aerodynamic Characteristics on the Spinning Motion of Aircraft," *Journal of Aircraft,* v. 8, no. 10 (October 1971), pp. 764-768.

[8] Bihrle, W., Jr., and Barnhart, B., "Departure Susceptibility and Uncoordinated Roll-Reversal Boundaries for Fighter Configurations," *Journal of Aircraft,* v. 19, no. 11 (November 1982), pp. 897-903.

[9] Moul, M.T., and Paulson, J.W., "Dynamic Lateral Behavior of High-Performance Aircraft," NACA Research Memorandum L58E16 (August 6, 1958).

[10] Weissman, R., "Preliminary Criteria for Predicting Departure Characteristics/Spin Susceptibility of Fighter-Type Aircraft," *Journal of Aircraft,* v. 10, no. 4 (April 1973), pp. 214-219.

[11] Mello, J., and Agnew, J., "MCAIR Design Philosophy for Fighter Aircraft Departure and Spin Resistance," SAE Paper no. 791081, SAE Aerospace Meeting, Los Angeles, CA (December 3-6, 1979).

[12] Skow, A.M., and Titiriga, A., Jr., "A Survey of Analytical and Experimental Techniques to Predict Aircraft Dynamic Characteristics at High Angles of Attack," *Dynamic Stability Parameters,* AGARD CP-235 (November 1978).

[13] Tinger, H.L., "Analysis and Application of Aircraft Departure Prediction Criteria to the AV-8B Harrier II," AIAA Paper no. 87-2561, AIAA Atmospheric Flight Mechanics Conference, Monterey, CA (August 1987).

[14] Titiriga, A., Jr., Ackerman, J.S., and Skow, A.M., "Design Technology for Departure Resistance of Fighter Aircraft," *Stall/Spin Problems of Military Aircraft,* AGARD CP-199 (June 1971).

[15] Pelikan, R.J., "F/A-18 High Angle of Attack Departure Resistant Criteria for Control Law Development," AIAA Paper no. 83-2126, AIAA Atmospheric Flight Mechanics Conference, Gatlinburg, TN (August 15-17, 1983).

[16] Kalviste, J., "Aircraft Stability Characteristics at High Angles of Attack," *Dynamic Stability Parameters,* AGARD CP-235 (May 1978).

[17] Balas, G.J., Doyle, J.C., Glover, K., Packard, A., and Smith, R., *μ-Analysis and Synthesis Toolbox: User's Guide,* The MathWorks, Inc.

[18] Gao, Z., and Antsaklis, P.J., "New Bounds on Parameter Uncertainties for Robust Stability," American Controls Conference, Boston, MA (June 1991), pp. 879-880.

[19] Latchman, H.A., and Letra, J.A., "On the Computation of Allowable Bounds for Parametric Uncertainty," American Controls Conference, Boston, MA (June 1991), pp. 867-868.

[20] Doyle, J.C., "Analysis of Feedback Systems with Structured Uncertainties," *IEE Proceedings,* Part D, v. 129, no. 6 (November 1982), pp. 242-250.

[21] Manning, M.K., and Banda, S.S., "Approximate Structured Singular Value Computation via Frobenius Norms," International Conference on Systems Engineering, Dayton, OH (August 24-26, 1989).

[22] Jones, R.D., "Structured Singular Value Analysis for Real Parameter Variations," AIAA 87-2589, AIAA Guidance, Navigation, and Control Conference, Monterey, CA (August 1987).

[23] Osborne, E.E., "On Pre-Conditioning of Matrices," *Journal of the Association for Computing Machinery,* v. 7, no. 4 (October 1960), pp. 338-345.

[24] Butler, R.W., and Langham, T.F., "Aircraft Motion Sensitivity to Variations in Dynamic Stability Parameters," *Dynamic Stability Parameters,* AGARD CP-235 (November 1978).

[25] Stein, G., and Henke, A.H., "A Design Procedure and Handling-Quality Criteria for Lateral-Directional Flight Control Systems," Technical Report AFFDL-TR-70-152 (February 1971).

[26] MATLAB™ — The MathWorks, Inc., Cochituate Place, 24 Prime Park Way, Natick, MA 01760.

[27] Brumbaugh, R.W., "An Aircraft Model for the AIAA Controls Design Challenge," AIAA 91-2631, AIAA Guidance, Navigation, and Control Conference, New Orleans, LA (August 1991).

[28] Stengel, R.F., and Berry, P.W., "Stability and Control of Maneuvering High-Performance Aircraft," NASA Contractor Report CR-2788 (April 1977).

[29] Kwakernaak, H., and Sivan, R., *Linear Optimal Control Systems,* John Wiley & Sons, Inc., New York, 1972, pp. 2-3.

[30] Roskam, J., *Airplane Flight Dynamics and Automatic Flight Controls, Part I,* Roskam Aviation and Engineering Corp., 1979, pp. 442-448.

[31] Gill, P.E., Murray, W., and Wright, M.H., *Practical Optimization,* Academic Press, Inc., San Diego, 1981, pp. 88-91.

7. Appendix: MATLAB™ Source Code

Appended below are several relevant MATLAB "M-files" used in the preparation of this thesis.

■ *SSV.M*

```
function mu = ssv(a,e,f,w)
%  SSV     Finds approx. structured singular value for supplied parameters.
%          This version only works for a 2x2 M matrix.  This algorithm
%          also uses Jones' formula for strictly real-valued parameter
%          variations.
%          SYNTAX: mu = ssv(a,e,f,w)
%              a = nominal A matrix
%              e,f = pre- and postmultiplier matrices
%              w = a frequency vector (one row)
%              mu = the vector of maximum structured singular values

% Check inputs:
m = f * inv(sqrt(-1) * eye(a) - a) * e;
[j,k] = size(m);
if (j ~= k), error('M matrix not square.'); end;
if (j ~= 2), error('M matrix not 2x2.'); end;
% Set up PHI_TOTAL:
phit = [-1 -1; -1 1; 1 -1; 1 1];
[j,k] = size(w);
% Do frequency sweep:
for i=1:k,
    m = f * inv(sqrt(-1) * w(1,i) * eye(a) - a) * e;
% Find scaling matrix:
    r = sqrt(sqrt((m(1,2)' * m(1,2)) / (m(2,1)' * m(2,1))));
    g = [1 0; 0 r] * m * [1 0; 0 1/r];
% Maximize over all possible phi vectors:
    for j=1:4,
        phi = diag(phit(j,:));
        s = svd((g*phi + (g*phi)')/2);
        svam(j) = s(1);
    end;
    mu(i) = max(svam);
end;
return;
```

■ *DPSRCH.M*

```
%  DPSRCH   Produces matrices DPSSV and SPEED, given vector WLIMIT (freq limits).
%           Uses two elements from the A matrix: drdot/dbeta, dpdot/dbeta.
%           Must have previously run THES_DAT and THES_TRM.  Only runs at points
%           inside the trim envelope defined by matrix TRIM.  DPSSV and SPEED
%           are of size(CNBDYN).  DPSSV contains the "size" of delta for each
%           point, while SPEED contains the period of the dynamics involved.
%               WLIMIT = [WLO WHI] (min freq, max freq of interest)

% Define tolerance for search routine:
TOL = 0.00005;
clear DPSSV SPEED;
% Check input and set up frequency vector:
if (size(WLIMIT) ~= [1 2]), error('WLIMIT is wrong size!'); end;
d1 = log10(WLIMIT(1));
d2 = log10(WLIMIT(2));
W = (10).^ [d1+(0:48)*(d2-d1) / 49, d2];
clear d1 d2;
% Define p as 2 * pi, gr as golden ratio:
p = 6.2832;
gr = (sqrt(5) - 1) / 2;
% Set up pre- and postmultiplier matrices:
C = zeros(2,10);
C(1,6) = 1;
C(2,6) = 1;
B = zeros(10,2);
ma = 0;
for a=ALP,
% Indices na and nb reference elements in the TRIM matrix.
    na = a/2 + 2;
% Indices ma and mb reference elements in the DPSSV and SPEED matrices.
    ma = ma + 1;
    mb = 0;
    for b=BTA,
        nb = b/2 + 18;
        mb = mb + 1;
% If aircraft was untrimmable, skip to next point:
        if (TRIM(na,nb) == 0),
            DPSSV(ma,mb) = 0;
            SPEED(ma,mb) = 0;
        else,
% Load relevant linearized A matrix:
            s = ['ap00bp00'];
            if (a < 0), s(2) = 'n'; end;
            if (abs(a) < 10),
                s(4) = int2str(abs(a));
            else,
                s(3:4) = int2str(abs(a));
            end;
            if (b < 0), s(6) = 'n'; end;
            if (abs(b) < 10),
```

```
                s(8) = int2str(abs(b));
            else,
                s(7:8) = int2str(abs(b));
            end;
            s2 = ['load ' path '\' s];
            eval(s2);
            m = eval(s);
            s = ['clear ' s];
            eval(s);
            [j,k] = size(m);
            m = m(4:j,:);
% Set up B as non-dimensionalizer:
            B(1,1) = m(1,6);
            B(3,2) = m(3,6);
% Find global maximum structured singular value:
            mu = ssv(m,B,C,W);
            [f0,i] = max(mu);
% Use golden section search to improve answer:
            if (i==1), pa = W(1);
            else, pa = W(i-1);
            end;
            if (i==50), pb = WLIMIT(2) * 1.1;
            else, pb = W(i+1);
            end;
            p0 = (1-gr) * (pb-pa) + pa;
            p1 = gr * (pb-pa) + pa;
            f0 = ssv(m,B,C,p0);
            f1 = ssv(m,B,C,p1);
            while (pb-pa) > TOL,
                if (f0 > f1),
                    pb = p1;
                    p1 = p0;
                    f1 = f0;
                    p0 = (1-gr) * (pb-pa) + pa;
                    f0 = ssv(m,B,C,p0);
                else,
                    pa = p0;
                    p0 = p1;
                    f0 = f1;
                    p1 = gr * (pb-pa) + pa;
                    f1 = ssv(m,B,C,p1);
                end;
            end;
% Store results:
            DPSSV(ma,mb) = 1 / f0;
            SPEED(ma,mb) = p / p0;
        end;
    end;
end;
% Clean up for exit (delete global matrices):
clear ma mb na nb a b j k i B C p s s2 gr W w pa pb p0 p1 f0 f1 mu TOL;
```

■ *THES_MAP.M*

```
function map = thes_map(ab,TRIM,w,path)
%  THES_MAP     Produces a map of stability of aircraft from linear models
%               extracted by FANGS by examining eigenvalues.
%               Format: map = THES_MAP(ab,TRIM,w,p)
%                   map = the 'map' matrix
%                   ab = limit vector [amin amax astep bmin bmax bstep]
%                   TRIM = a trim map as produced by THES_TRM
%                   w = minimum frequency of interest; all eigenvalues with
%                       imaginary part less than w are discarded
%                   p = directory where .MAT files are located (a string)

[j,k] = size(ab);
if ((j ~= 1)|(k ~= 6)), error('Vector AB is incorrect size.'); end;
% Set value to store in map for nontrimmable points:
notrimval = 0;
ma = 0;
for a=ab(1):ab(3):ab(2),
% Indices na and nb reference elements in the TRIM matrix.
    na = a/2 + 2;
% Indices ma and mb reference elements in the DPSSV and SPEED matrices.
    ma = ma + 1;
    mb = 0;
    for b=ab(4):ab(6):ab(5),
        nb = b/2 + 18;
        mb = mb + 1;
% If aircraft was untrimmable, skip to next point:
        if (TRIM(na,nb) == 0),
            map(ma,mb) = notrimval;
        else,
% Load relevant linearized A matrix:
            s = ['ap00bp00'];
            if (a < 0), s(2) = 'n'; end;
            if (abs(a) < 10),
                s(4) = int2str(abs(a));
            else,
                s(3:4) = int2str(abs(a));
            end;
            if (b < 0), s(6) = 'n'; end;
            if (abs(b) < 10),
                s(8) = int2str(abs(b));
            else,
                s(7:8) = int2str(abs(b));
            end;
            s2 = ['load ' path '\' s];
            eval(s2);
            m = eval(s);
            s = ['clear ' s];
            eval(s);
            [j,k] = size(m);
            if (j ~= (k+3)),
```

```
                error(['Matrix ' s ' (less trim indicators) is not square!']);
            end;
            m = m(4:j,:);
% Get eigenvalues from A matrix:
            e = eig(m);
            f = real(e);
            g = imag(e);
            [j,k] = size(f);
% Check the eigenvalues:
            for c=1:j,
% If aperiodic with real part positive and less than 0.25, discard:
                if (g(c) == 0) & (f(c) >= 0) & (f(c) < 0.25),
                    f(c) = -100;
                end;
% If periodic with frequency less than cutoff given in function arguments, discard:
                if (abs(g(c)) < w) & (g(c) ~= 0),
                    f(c) = -100;
                end;
            end;
% Store real part of least stable remaining eigenvalue in output matrix:
            map(ma,mb) = max(f);
        end;
    end;
end;
return;
```

8. Vita

The author was born on April 19, 1969, in Jackson, Tennessee. He graduated from Crockett County High School in May, 1987, and entered Tennessee Technological University, Cookeville, Tennessee, in August of that year. He was awarded the Bachelor of Science degree in Physics in May, 1991, and was subsequently admitted to the aerospace engineering program at Virginia Polytechnic Institute and State University in August, 1991.